Electronic Supplementary Information (ESI)

Evolving Bifacial Molecule Strategy for Surface Passivation of Lead Halide Perovskite Solar Cells

Nanaki Minoi,[a] *Fumitaka Ishiwari,*[*,a,b,c] *Takuya Omine,*[a] *Kazuharu Murotani,*[a] *Ryosuke Nishikubo,*[a,b] *and Akinori Saeki*[*,a,b]

[a] Department of Applied Chemistry, Graduate School of Engineering, Osaka University, 2-1 Yamadaoka, Suita, Osaka 565-0871, Japan.

[b] Innovative Catalysis Science Division, Institute for Open and Transdisciplinary Research Initiatives (ICS-OTRI), Osaka University, 1-1 Yamadaoka, Suita, Osaka 565-0871, Japan.

[c] PRESTO, Japan Science and Technology Agency (JST), Kawaguchi, Saitama 332-0012, Japan.

AUTHOR INFORMATION

Corresponding Author

*ishiwari@chem.eng.osaka-u.ac.jp (F.I.); saeki@chem.eng.osaka-u.ac.jp (A.S.)

This supporting information presents the following contents.

Experimental

Materials.

Chemicals for the synthesis of passivation molecules were purchased from Sigma-Aldrich or Tokyo Chemical Co. Ltd (TCI). Solvents for the synthesis were purchased from Kishida Kagaku Co. Ltd, Kanto Kagaku Co. Ltd, or Wako-Fuji Film Industries Ltd (WFFI) and used as received. Deoxidized grade dimethyl sulfoxide (DMSO), toluene, and *o*-dichlorobenzene (DCB) were purchased form WFFI and used as received. The highest grade chlorobenzene (CB) was purchased from Sigma-Aldrich and used as received. TRX-*syn* and TRX-*anti* were prepared according to the previously reported procedure.[S1] Perovskite precursors were purchased from TCI and used without further purification.

Scheme S1. Synthesis of PM-*anti* and PM-*syn*.[a]

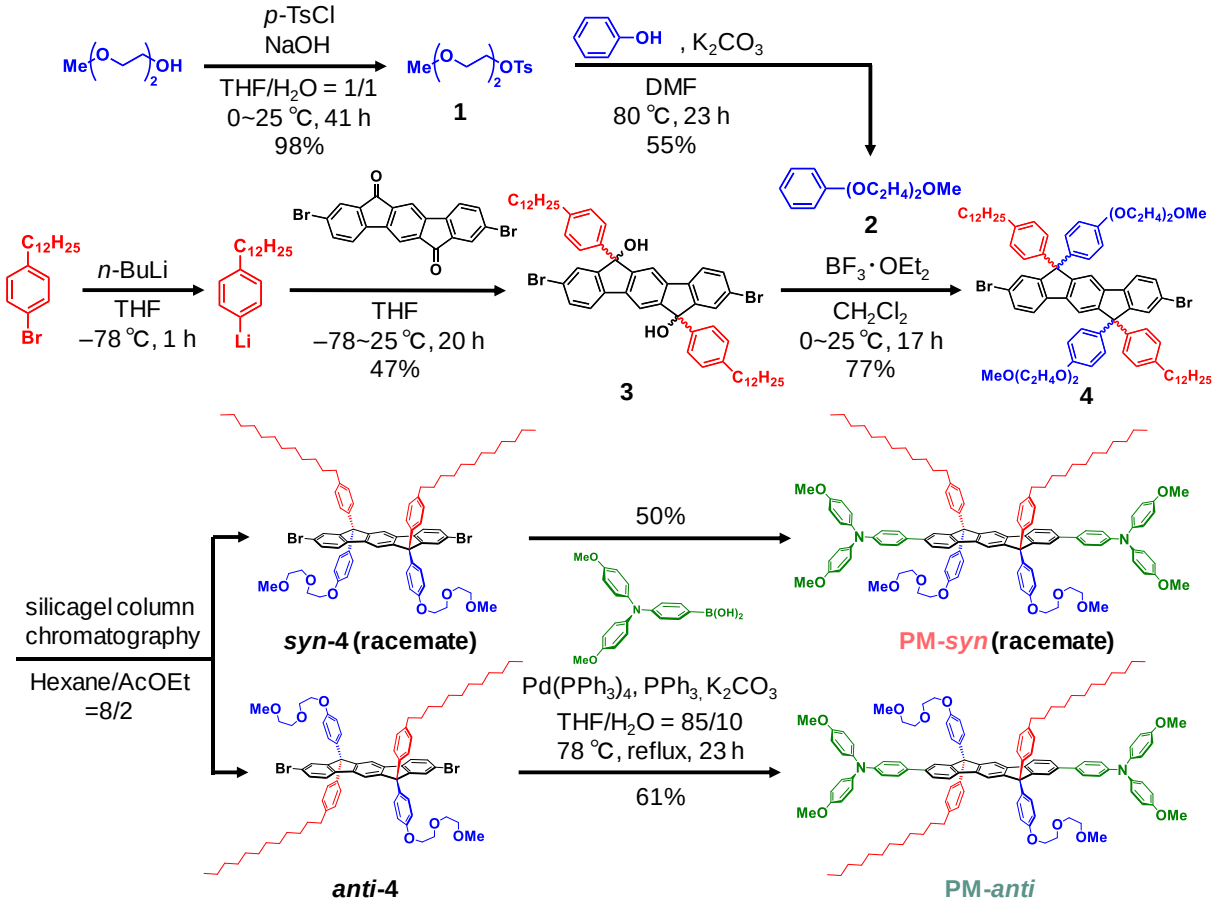

[a] For *syn*-compounds, the structures of only single enantiomers are shown.

Synthesis of compound 1

Diethylene glycol monomethyl ether (10.0 g, 83.2 mmol, 1.0 eq), NaOH (17.3 g, 432.8 mmol, 5.2 eq), *p*-TsCl (20.6 g, 108.2 mmol, 1.3 eq), THF (100 mL), and water (100 mL) were added to a 300 mL three-necked flask under nitrogen atmosphere. Then the mixture was cooled to 0 ℃ and stirred for 41 h. After that, it was quenched with HCl aq (10%) and extracted with $CHCl_3$. After it was washed with water and brine and dried with anhydrous $MgSO_4$, the solvent was removed under reduced pressure. As a result, compound 1 was obtained (22.6 g, 81.9 mmol, 98%). ^{1}H NMR (400 MHz, $CDCl_3$, **Fig. S1**) δ (ppm): 7.76 (d, J = 8.0 Hz, 2H), 7.30 (d, J = 8.0 Hz, 2H), 4.13 (t, J = 4.8 Hz, 2H), 3.65 (t, J = 4.8 Hz, 2H), 3.55-3.52 (m, 2H), 3.45-3.43 (m, 2H), 3.31 (s, 3H), 2.41 (s, 3H).

Synthesis of compound 2

Compound 1 (20.0 g, 72.9 mmol, 1.0 eq), phenol (6.9 g, 72.9 mmol, 1.0 eq), K_2CO_3 (22.7 g, 164.0 mmol, 2.25 eq) and DMF (80 mL) were added to a 200 mL two-necked flask under nitrogen atmosphere. Then the mixture was heated to 80 ℃ and stirred for 23 h. After that, it was quenched with HCl aq (10%) and extracted with diethylether. After it was washed with water and brine and dried with anhydrous $MgSO_4$, the solvent was removed under reduced pressure and the residue was purified by silicagel column chromatography (hexane/ethyl acetate = 8/2). As a result, compound 2 was obtained (7.8 g, 40.0 mmol, 55%). ^{1}H NMR (400 MHz, $CDCl_3$, **Fig. S2**) δ (ppm): 7.28 (t, J = 7.6 Hz, 2H), 6.96-6.91 (m, 3H), 4.15 (t, J = 5.0 Hz, 2H), 3.86 (t, J = 5.0 Hz, 2H), 3.74-3.72 (m, 2H), 3.59-3.57 (m, 2H), 3.40 (s, 3H).

Synthesis of compound 3 [S2]

1-bromo-4-dodecylbenzene (2.0 g, 5.9 mmol, 2.6 eq) and anhydrous THF (15 mL) were added to a 50 mL two-necked flask under nitrogen atmosphere. Then the mixture was cooled to –78 ℃ and *n*-buthyllithium (*n*-BuLi) (2.2 mL, 5.7 mmol, 2.5 eq) was added to it. After it was stirred for 1 h, 2.8-dibromoindeno-[1,2-b]fluorene-6,12-dione (1.0 g, 2.3 mmol, 1.0 eq) was added to it and it was stirred for 20 h while raising the temperature to room temperature. After that, it was quenched with water and unreacted 2,8-dibromo-[1,2-b]fluorene-6,12-dione was separated by vacuum filtration. The residue was extracted with ethyl acetate. After it was washed with water and brine and dried with anhydrous $MgSO_4$, the solvent was removed under reduced pressure and the residue was purified by silicagel column chromatography (hexane/chloroform = 3/7). As a result, compound 3 was obtained (1.1 g, 1.1 mmol, 47%). ^{1}H NMR (600 MHz, DMSO-d_6, **Fig. S3**) δ (ppm): 7.79 (d, J = 8.0 Hz, 2H), 7.69 (s, 2H), 7.50 (dd, J = 8.0, 1.9 Hz, 2H), 7.30 (s, 2H), 7.19 (d, J = 8.1 Hz, 4H), 7.09 (d, J = 8.1 Hz, 4H), 6.49 (s, 2H), 1.50 (t, J = 6.7 Hz, 4H), 1.25-1.22 (m, 36H), 0.84 (t, J = 6.9 Hz, 4H).

Synthesis of compound 4

Compound 3 (0.70 g, 0.76 mmol, 1.0 eq), compound 2b (0.59 g, 3.0 mmol, 4.0 eq), and anhydrous CH_2Cl_2 (10 mL) was added to a 50 mL two-necked flask under nitrogen atmosphere. Then the mixture was cooled to 0 ℃ and $BF_3 \cdot OEt_2$ (0.38 mL, 3.0 mmol, 4.0 eq) was added to it. Then it was stirred for 17 h while raising the temperature to room temperature. After that, it was quenched with water and extracted with $CHCl_3$. After it was dried with anhydrous $MgSO_4$, the solvent was removed under reduced pressure. The residue was purified and separated into *syn*-4 and *anti*-4 by silicagel column chromatography (hexane/ethyl acetate = 8/2). As a result, compound 4 was obtained (0.75 g, 0.59 mmol, 77%). ^{1}H NMR of *syn*-4 (600 MHz, $CDCl_3$, **Fig. S4**) δ (ppm): 7.68 (s, 2H), 7.51-7.50 (m, 4H), 7.46, (s, 2H), 7.42 (dd, J = 8.4, 1.2 Hz, 2H), 7.15 (d, J = 9.0 Hz, 8H), 7.09 (d, J = 8.1 Hz, 4H), 6.83 (d, J = 8.1 Hz, 4H), 4.12 (t, J = 4.8 Hz, 4H), 3.85 (t, J = 4.8 Hz, 4H), 3.72 (t, J = 4.8 Hz 4H), 3.58 (t, J = 4.8 Hz 4H), 3.40 (s, 6H), 2.58 (t, J = 7.8 Hz, 4H), 1.61 (q, J = 7.5 Hz, 4H), 1.33-1.28 (m, 36H), 0.91 (t, J = 6.9 Hz, 6H). ^{13}C NMR of *syn*-4 (125 MHz, $CDCl_3$, **Fig. S5**) δ (ppm): 157.8, 154.2, 151.5, 142.5, 141.7, 139.4, 138.9, 137.6, 130.6, 129.4, 129.3, 128.5, 128.1, 121.6, 121.3, 117.8, 114.5, 72.1, 70.8, 69.8, 67.4, 64.5, 59.2, 35.6, 32.0, 31.5, 29.8, 29.7, 29.7, 29.6, 29.6, 29.5, 22.8, 14.2. FT-IR of *syn*-4 (KBr, **Fig. S6**) ν (cm^{-1}): 2922, 2852, 2360, 1608, 1508, 1455, 1422, 1295, 1251, 1181, 1112, 1063, 933, 868, 821, 742, 672, 630, 521. High-Resolution MALDI-TOF-MS of *syn*-4 (**Fig. S7**): calcd. for $C_{78}H_{96}O_6Br_2$, m/z = 1286.56, found 1286.56. ^{1}H NMR of *anti*-4 (600 MHz, $CDCl_3$, **Fig. S8**) δ (ppm): 7.66 (s, 2H), 7.50 (d, J = 8.4 Hz, 2H), 7.48, (d, J = 1.8 Hz, 2H), 7.41 (dd, J = 8.4, 1.8 Hz, 2H), 7.13 (dd, J = 8.4, 2.7 Hz, 8H), 7.07 (d, J = 8.4 Hz, 4H), 6.81 (d, J = 8.4 Hz, 4H), 4.11 (t, J = 4.8 Hz, 4H), 3.84 (t, J = 4.8 Hz, 4H), 3.72-3.70 (m, 4H), 3.57-3.56 (m, 4H), 3.38 (s, 6H), 2.57 (t, J = 7.8 Hz), 1.60 (q, J = 7.2 Hz, 4H), 1.33-1.27 (m, 36H), 0.89 (t, J = 7.2 Hz, 6H). ^{13}C NMR of *anti*-4 (125 MHz, $CDCl_3$, **Fig. S9**) δ (ppm): 157.8, 154.2, 151.6, 142.5, 141.8, 139.4, 139.0, 137.6, 130.62, 129.40, 129.37, 128.5, 128.1, 121.6, 121.4, 117.9, 114.5, 72.1, 70.8, 69.8,

67.5, 64.5, 59.2, 35.7, 32.0, 31.5, 29.8, 29.8, 29.7, 29.6, 29.5, 22.8, 14.3. FT-IR of *anti*-4 (KBr, **Fig. S10**) ν (cm^{-1}): 2925, 2853, 2361, 1608, 1508, 1457, 1422, 1294, 1251, 1181, 1113, 1063, 932, 868, 820, 742, 672, 630, 526. High-Resolution MALDI-TOF-MS of *anti*-4 (**Fig. S11**): calcd. for $C_{78}H_{96}O_6Br_2$, *m*/*z* = 1286.56, found 1286.56.

Synthesis of PM-*syn*

syn-4 (0.30 g, 0.23 mmol, 1.0 eq), [4-[bis(4-methoxyphenyl)amino]phenyl]boronic acid (0.65 g, 1.9 mmol, 8.0 eq), K_2CO_3 (3.8 g, 27.6 mmol, 120 eq), PPh_3 (0.029 g, 0.11 mmol, 0.48 eq), $Pd(PPh_3)_4$ (0.060 g, 0.055 mmol, 0.24 eq), THF (15 mL) and water (1.8 mL) were added to a 50 mL two-necked flask under nitrogen atmosphere. Then the mixture was refluxed for 23 h at 78 ℃. After that, it was quenched with water and extracted with $CHCl_3$. After it was washed with water and dried with anhydrous $MgSO_4$, the solvent was removed under reduced pressure. The residue was purified by silicagel column chromatography (ethyl acetate) and HPLC chiral column chromatography (Daicel CHIRALPAK IE-3, hexane/ethyl acetate = 8/2). As a result, PM-*syn* was obtained (0.20 g, 0.12 mmol, 50%). ^{1}H NMR (600 MHz, $CDCl_3$, **Fig. S12**) δ (ppm): 7.71 (s, 2H), 7.67 (d, *J* = 7.8 Hz, 2H), 7.51 (d, *J* = 1.2 Hz, 2H), 7.49 (dd, *J* = 7.8, 1.2 Hz, 2H), 7.37 (d, *J* = 9.0 Hz, 4H), 7.20 (dd, *J* = 9.0, 2.4 Hz, 8H), 7.06 (d, *J* = 9.0 Hz, 8H), 7.05 (d. *J* = 9.0 Hz, 4H), 6.95 (d. *J* = 9.0 Hz, 4H), 6.83 (d, *J* = 9.0 Hz, 8H), 6.79, (d, *J* = 9.0 Hz, 4H), 4.09 (t, *J* = 5.1 Hz, 4H), 3.82 (t, *J* = 5.1 Hz, 4H), 3.80 (s, 12H), 3.70 (t, *J* = 4.8 Hz, 4H), 3.55 (t, *J* = 4.8 Hz, 4H), 3.37 (s, 6H), 2.54 (t, *J* = 7.8 Hz, 4H), 1.57 (q, *J* = 6.0 Hz, 4H), 1.34-1.25 (m, 36H), 0.87 (t, *J* = 7.2 Hz, 6H). ^{13}C NMR (125 MHz, $CDCl_3$, **Fig. S13**) δ (ppm): 157.6, 156.0, 152.8, 151.8, 148.2, 143.5, 141.4, 141.0, 140.0, 139.8, 138.7, 138.7, 133.4, 129.6, 128.3, 128.3, 127.6, 126.6, 125.8, 124.2, 120.9, 120.4, 117.7, 114.8, 114.3, 72.1, 70.8, 69.9, 67.4, 64.4, 59.2, 55.6, 35.7, 32.1, 31.5, 29.8, 29.8, 29.8, 29.7, 29.7, 29.7, 29.5, 22.8, 14.3. FT-IR (KBr, **Fig. S14**) ν (cm^{-1}): 2925, 2853, 1604, 1506, 1459, 1439, 1318, 1283, 1242, 1179, 1108, 1037, 925, 823, 676, 580, 520. High-Resolution MALDI-TOF-MS (**Fig. S15**): calcd. for $C_{118}H_{132}N_2O_{10}$, *m*/*z* = 1736.99, found 1736.99.

Synthesis of PM-*anti*

Anti-4 (0.15 g, 0.12 mmol, 1.0 eq), [4-[bis(4-methoxyphenyl)amino]phenyl]boronic acid (0.32 g, 0.93 mmol, 8.0 eq), K_2CO_3 (1.9 g, 13.8 mmol, 120 eq), PPh_3 (0.015 g, 0.055 mmol, 0.48 eq), $Pd(PPh_3)_4$ (0.030 g, 0.028 mmol, 0.24 eq), THF (15 mL) and water (1.8 mL) were added to a 50 mL two-necked flask under nitrogen atmosphere. Then the mixture was refluxed for 23 h at 78 ℃. After that, it was quenched with water and extracted with $CHCl_3$. After it was washed with water and dried with anhydrous $MgSO_4$, the solvent was removed under reduced pressure. The residue was purified by silicagel column chromatography (ethyl acetate) and HPLC chiral column chromatography (Daicel CHIRALPAK IE-3, hexane/ethyl acetate = 8/2). As a result, PM-*anti* was obtained (0.12 g, 0.070 mmol, 61%). ^{1}H NMR (600 MHz, $CDCl_3$, **Fig. S16**) δ (ppm): 7.72 (s, 2H), 7.67 (d, *J* = 7.8 Hz, 2H), 7.53 (s, 2H), 7.50 (d, *J* = 7.8 Hz, 2H), 7.37 (d, *J* = 7.8 Hz, 4H), 7.21 (d, *J* = 9.0 Hz, 4H), 7.20 (d, *J* = 9.0 Hz, 4H), 7.07-7.04 (m, 12H), 6.95 (d. *J* = 7.2 Hz, 4H), 6.83 (d, *J* = 9.0 Hz, 8H), 6.79, (d, *J* = 9.0 Hz, 4H), 4.10 (t, *J* = 5.1 Hz, 4H), 3.83 (t, *J* = 5.1 Hz, 4H), 3.80 (s, 12H), 3.70 (m, 4H), 3.55 (m, 4H), 3.37 (s, 6H), 2.55 (t, *J* = 7.8 Hz, 4H), 1.58 (q, *J* = 7.8 Hz, 4H), 1.34-1.25 (m, 36H), 0.88 (t, *J* = 7.2 Hz, 6H). ^{13}C NMR (125 MHz, $CDCl_3$, **Fig. S17**) δ (ppm): 157.6, 156.0, 152.8, 151.8, 148.1, 143.5, 141.4, 141.0, 140.0, 139.8, 138.7, 138.7, 133.4, 129.6, 128.3, 128.3, 127.6, 126.6, 125.8, 124.2, 120.9, 120.4, 117.7, 114.8, 114.4, 72.1, 70.8, 69.9, 67.4, 64.4, 59.2, 55.6, 35.7, 32.1, 31.5, 29.8, 29.8, 29.8, 29.7, 29.7, 29.7, 29.5, 22.8, 14.3. FT-IR (KBr, **Fig. S18**) ν (cm^{-1}): 2925, 2853, 1604, 1507, 1458, 1439, 1318, 1283, 1242, 1179, 1108, 1037, 823, 724, 679, 581, 545. High-Resolution MALDI-TOF-MS (**Fig. S19**): calcd. for $C_{118}H_{132}N_2O_{10}$, *m*/*z* = 1736.99, found 1736.99. Chiral HPLC charts of *syn*-PM and *anti*-PM was shown in **Fig. S20**.

Hole-only space-charge-limited current (SCLC) device

An ITO/glass substrate was washed by sonication with acetone and isopropanol for more than 15 min each, and treated by O_3/ultraviolet for more than 15 min. Then, a PEDOT:PSS solution (300 μL) was spin-coated at 5000 rpm for 60 s and thermal annealed at 120 °C for 30 min. Then, a chlorobenzene solution of passivation molecule (60 mg mL^{-1}) (50 μL) was spin-coated at 4000 rpm for 15 s. Finally, 70 nm Au layer was deposited by vacuum evaporation through a shadow mask (area: 7.07 mm^2). Current-voltage curves were measured using a source-meter unit (ADCMT Corp., 6241A) in darkness.

Theoretical calculation

Density functional theory (DFT) calculations were performed using Gaussian 16 program package.[S3] The geometry optimizations were performed at the B3LYP/6-31G(d) level of calculations in vacuum. Optimized geometries were verified by frequency computations as minima (no imaginary frequencies) or transition structures (one imaginary frequency).

Supporting Tables

Table S1. Summary of TRPL analyses.[a]

Sample	τ_1 / ns (intensity / %)	τ_2 / ns (intensity / %)	τ_{ave} / ns
PVK	257.2 (32.6)	1506.3 (67.4)	1099.0
PVK/PM$_{prev}$-*syn*[b]	139.0 (67.7)	1193.6 (32.3)	479.4
PVK/PM$_{prev}$-*anti*[b]	237.0 (58.5)	1038.7 (41.5)	569.9
PVK/PM-*syn*	23.2 (53.7)	249.0 (46.3)	127.7
PVK/PM-*anti*	41.1 (71.1)	477.0 (28.9)	167.2
PVK[c]	54.4 (62.6)	2862.0 (37.4)	1103.1
PVK/TRX-*syn*	31.7 (45.3)	2164.8 (54.7)	1197.8
PVK/TRX-*syn*	40.6 (56.1)	2039.1 (43.9)	918.7

[a]Fitted by double exponential functions: $f(t) = A_1 exp\left(-\frac{t}{\tau_1}\right) + A_2 exp\left(-\frac{t}{\tau_2}\right)$. Average lifetime = $(A_1\tau_1 + A_2\tau_2)(A_1 + A_2)^{-1}$. [b]Taken from reference S2. [c] The reference sample (PVK) for the TRX-treated samples.

Table S2. Summary of TRMC analyses.[a]

Sample	τ_1 / ns (intensity / %)	τ_2 / ns (intensity / %)	τ_{ave} / ns
mp-TiO$_2$/PVK	1422 (55.4)	15546 (44.6)	7723
mp-TiO$_2$/PVK/ PM$_{prev}$-*syn*[b]	602 (95.1)	7911 (4.9)	959
mp-TiO$_2$/PVK/ PM$_{prev}$-*anti*[b]	749 (84.9)	10384 (15.1)	2201
mp-TiO$_2$/PVK/PM-*syn*	383 (91.9)	2965 (8.1)	594
mp-TiO$_2$/PVK/PM-*anti*	562 (82.3)	2335 (17.7)	876
mp-TiO$_2$/PVK[c]	1504 (64.0)	26680 (36.0)	10560
mp-TiO$_2$/PVK/TRX-*syn*	1148 (58.3)	27391 (41.7)	12085
mp-TiO$_2$/PVK/TRX-*anti*	1103 (59.2)	21504 (40.8)	9436

[a]Fitted by double exponential functions: $f(t) = A_1 exp\left(-\frac{t}{\tau_1}\right) + A_2 exp\left(-\frac{t}{\tau_2}\right)$. Average lifetime = $(A_1\tau_1 + A_2\tau_2)(A_1 + A_2)^{-1}$. [b]Taken from reference S2. [c] The reference sample (mp-TiO$_2$/PVK) for the TRX-treated samples.

Table S3. Summary of hole-only SCLC measurements of PM.[a]

Sample	Doping	μ_h / cm^2 V^{-1} s^{-1}	L / nm
spiro-OMeTAD	–	5.1×10^{-5}	70
	doped	1.2×10^{-3}	68
PM-*syn*	–	9.9×10^{-6}	93
	doped	1.1×10^{-3}	95
PM-*anti*	–	4.8×10^{-6}	82
	doped	9.2×10^{-4}	94

[a] ITO/PEDOT:PSS/active layer/Au. The active layer was spin-coated from CB solution of 78.2 mg mL^{-1}.

Table S4. Summary of PSC devices with/without passivation at different conccentrations.[a]

Passivation	c / mg mL^{-1} [b]	PCE / %	J_{SC} / mA cm^{-2}	V_{OC} / V	FF	HI[c]	Device No.
PM-*syn*	1.0	16.19±0.21 (17.58)	24.35±0.29 (24.74)	0.958±0.009 (0.963)	0.694±0.004 (0.738)	0.11±0.03 (0.10)	6
	3.0	16.85±0.34 (18.79)	24.20±0.52 (24.84)	0.990±0.007 (1.013)	0.703±0.010 (0.747)	0.11±0.04 (0.07)	6
	5.0	16.47±0.58 (18.47)	24.31±0.29 (24.25)	0.984±0.014 (0.996)	0.688±0.014 (0.750)	0.15±0.06 (0.13)	6
PM-*anti*	1.0	16.91±0.33 (18.38)	24.21±0.44 (24.66)	0.986±0.008 (0.995)	0.708±0.003 (0.749)	0.09±0.03 (0.12)	6
	3.0	17.01±0.39 (18.71)	24.41±0.38 (24.92)	0.985±0.012 (1.008)	0.707±0.004 (0.745)	0.08±0.04 (0.11)	6
	5.0	16.34±1.08 (18.27)	23.64±1.37 (24.82)	1.001±0.011 (1.002)	0.691±0.026 (0.735)	0.05±0.10 (0.17)	6
TRX-*syn*	0.5	18.09±0.43 (19.76)	24.79±0.42 (25.47)	1.038±0.006 (1.051)	0.703±0.007 (0.738)	0.09±0.04 (0.10)	6
	1.0	17.33±0.31 (18.88)	24.99±0.40 (25.52)	1.017±0.012 (1.031)	0.682±0.005 (0.718)	0.15±0.03 (0.13)	8
	2.0	15.94±0.66 (18.26)	23.97±1.07 (24.47)	0.993±0.009 (1.023)	0.670±0.011 (0.729)	0.18±0.07 (0.16)	7
	3.0	14.69±0.81 (17.15)	23.18±1.19 (24.26)	0.977±0.006 (0.994)	0.648±0.023 (0.711)	0.22±0.10 (0.18)	8
TRX-*anti* [c]	0.5	16.66±0.57 (18.70)	24.83±0.42 (25.32)	0.997±0.007 (1.011)	0.672±0.016 (0.731)	0.19±0.06 (0.17)	8
	1.0	17.06±0.49 (18.86)	24.79±0.44 (25.32)	1.005±0.004 (1.016)	0.684±0.011 (0.733)	0.17±0.06 (0.20)	8
	2.0	16.37±0.57 (18.44)	24.47±0.62 (25.33)	1.002±0.007 (1.004)	0.667±0.011 (0.725)	0.18±0.06 (0.16)	7
	3.0	15.82±0.38 (17.73)	24.47±0.52 (25.26)	0.994±0.004 (0.999)	0.650±0.010 (0.706)	0.16±0.04 (0.18)	6

[a] FTO/mpTiO_2/$MA_{0.13}FA_{0.87}PbI_{2.61}Br_{0.39}$/passivation/spiro-OMeTAD(doped)/Au under 1 sun (100 mW cm^{-2}). Values in parentheses are the maximum values. The average values were calculated over forward and reverse scans in multiple devices. The error values are the standard deviations of multiple devices over the forward and reverse scans. [b] Concentration in CB (PM) and IPA (TRX). [c] Hysteresis index (HI) = (reverse PCE – forward PCE)/(reverse PCE). [c] The best PCEs of TRX-*anti* 0.5 and 1.0 mg mL^{-1} were very similar, so that the former was shown in the main text for the consistency with the optimal concentration of TRX-*syn* (0.5 mg mL^{-1})

Supporting Figures

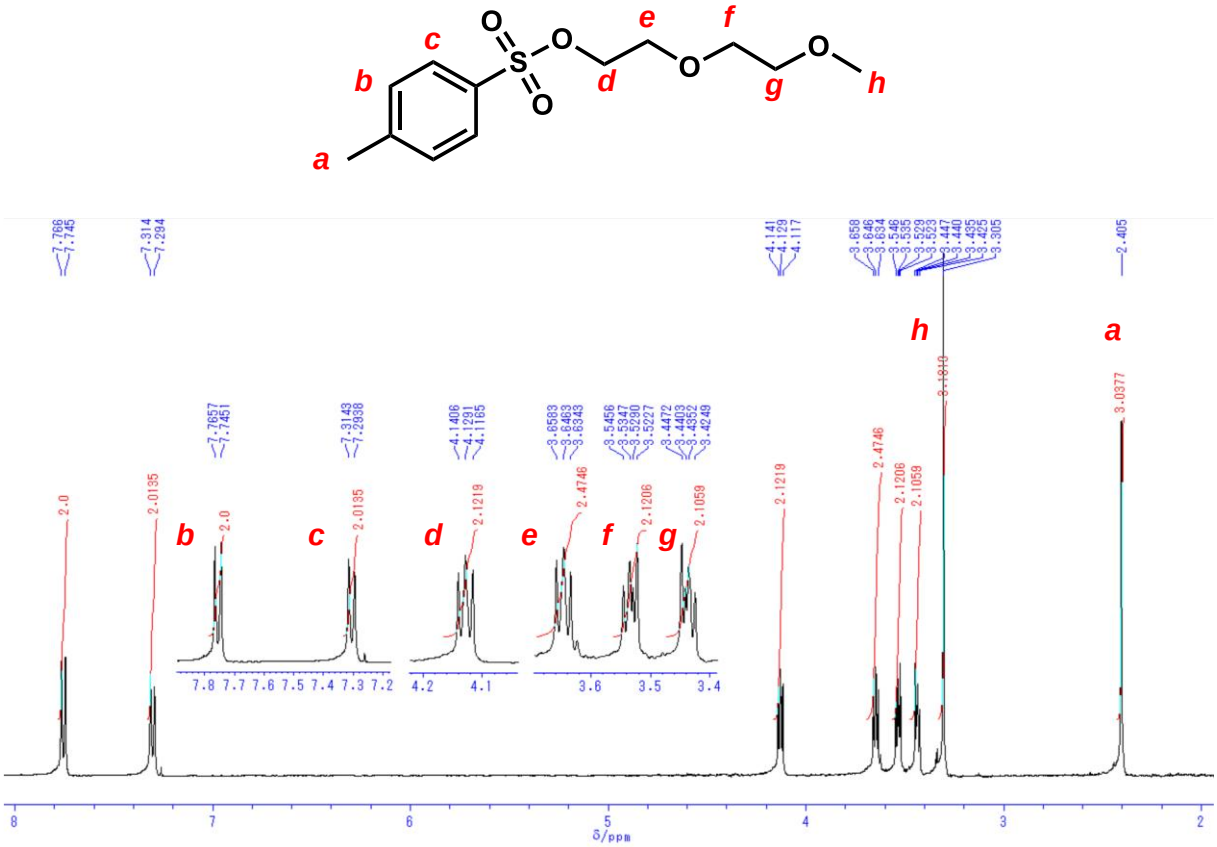

Figure S1. ^{1}H NMR spectrum of **1** (400 MHz, $CDCl_3$ at 25 °C).

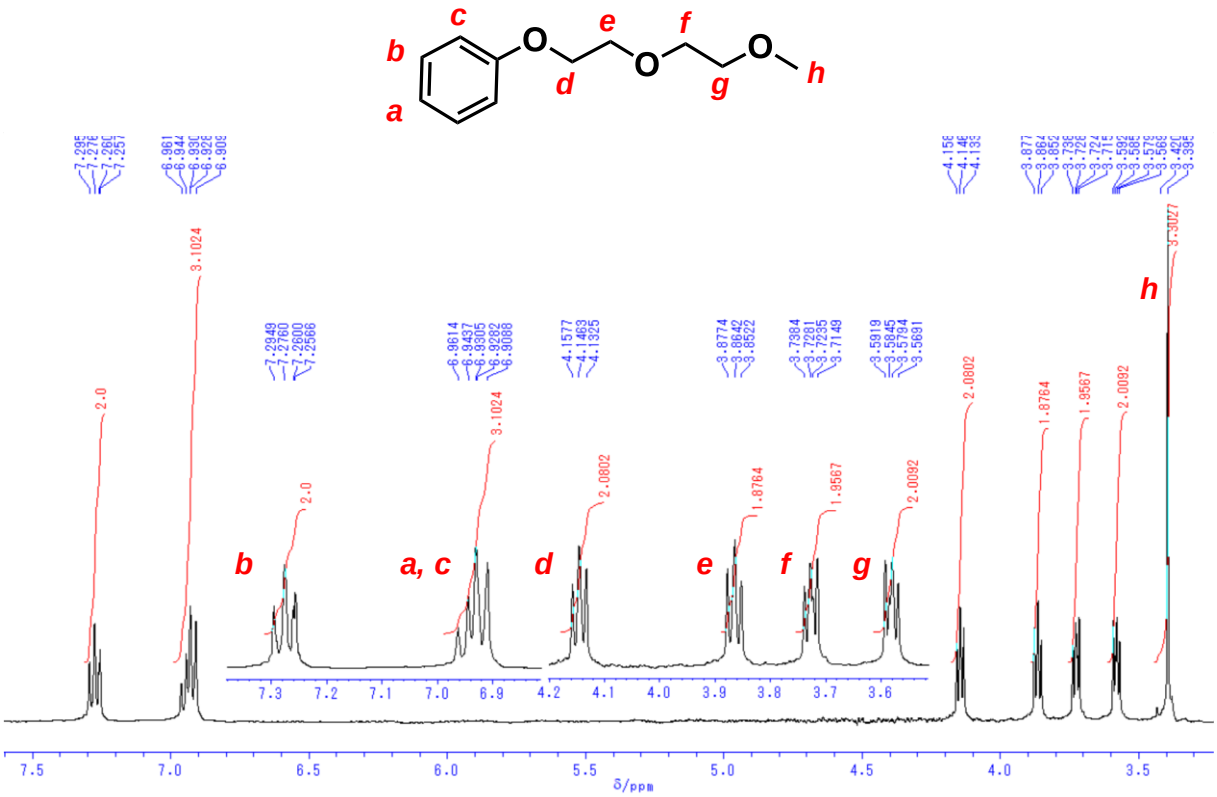

Figure S2. ^{1}H NMR spectrum of **2** (400 MHz, $CDCl_3$ at 25 °C).

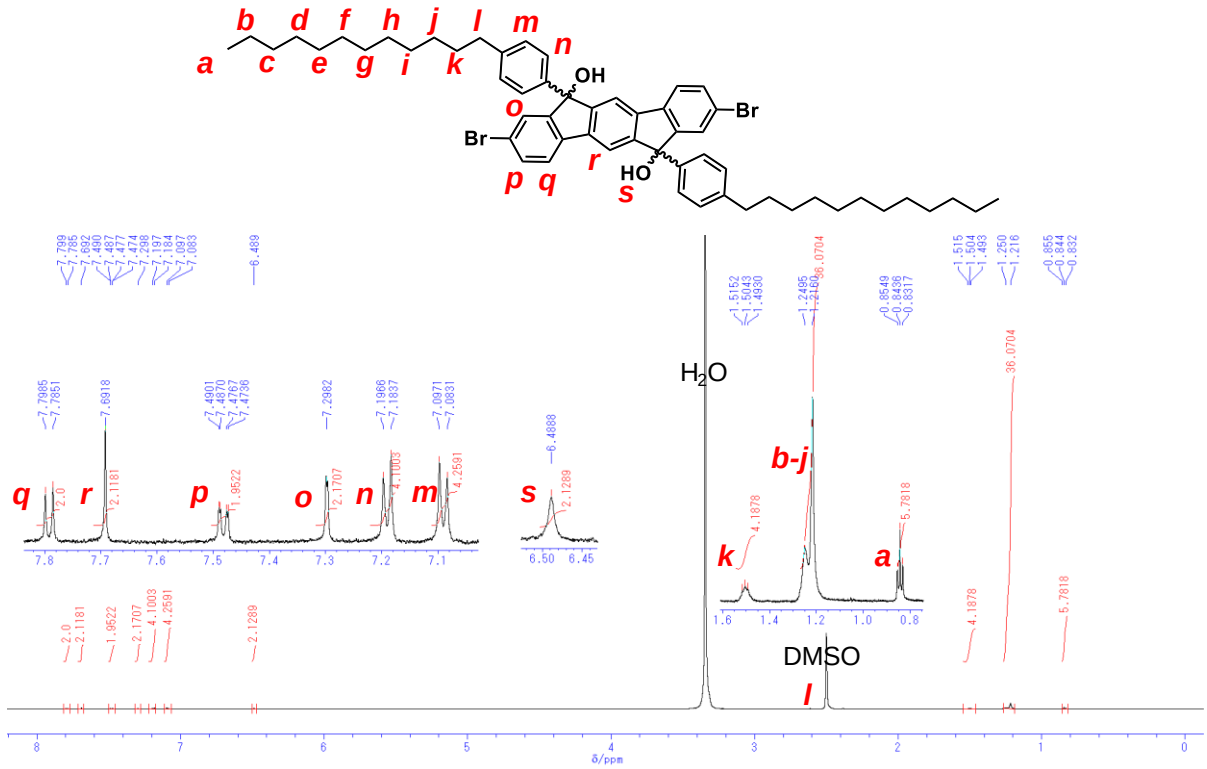

Figure S3. ^{1}H NMR spectrum of **3** (600 MHz, DMSO-d_6 at 25 °C).

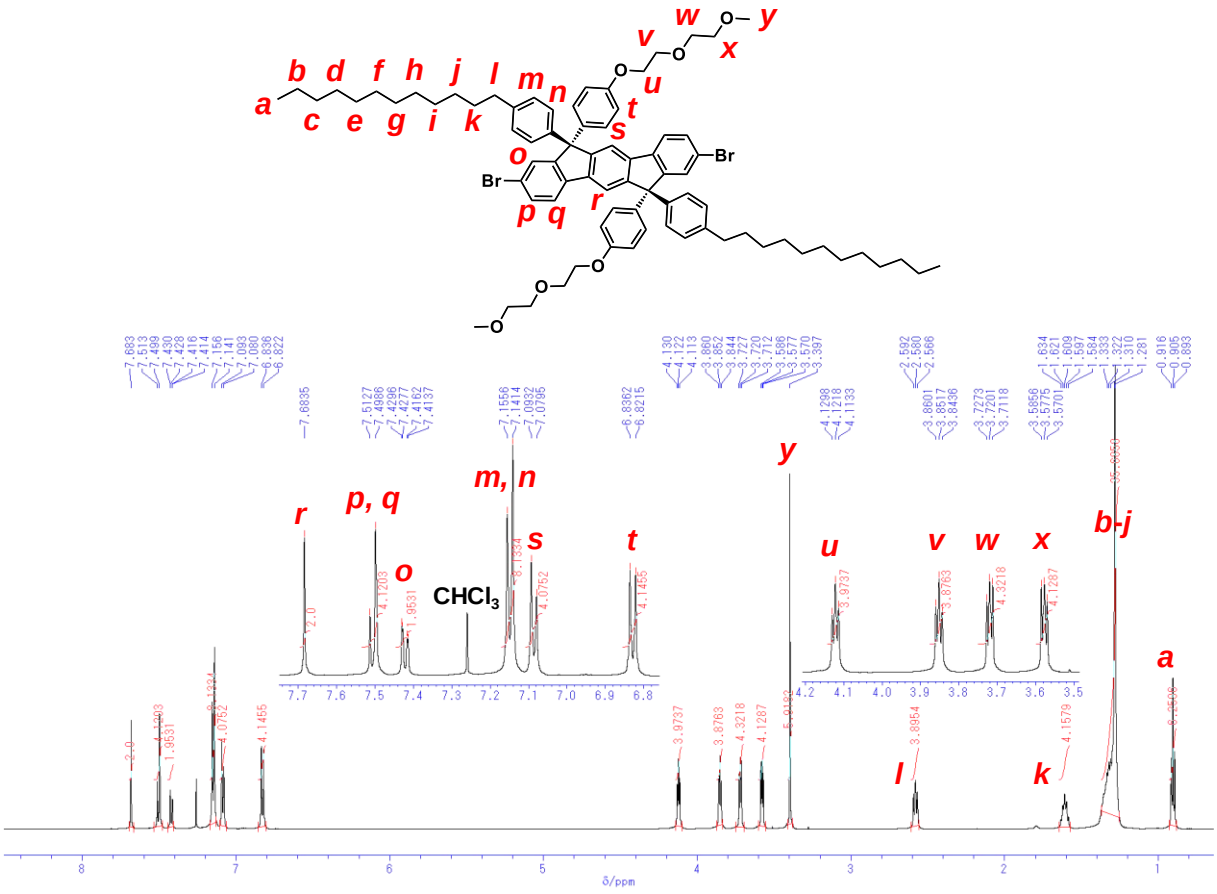

Figure S4. ^{1}H NMR spectrum of ***syn*-4** (600 MHz, $CDCl_3$ at 25 °C).

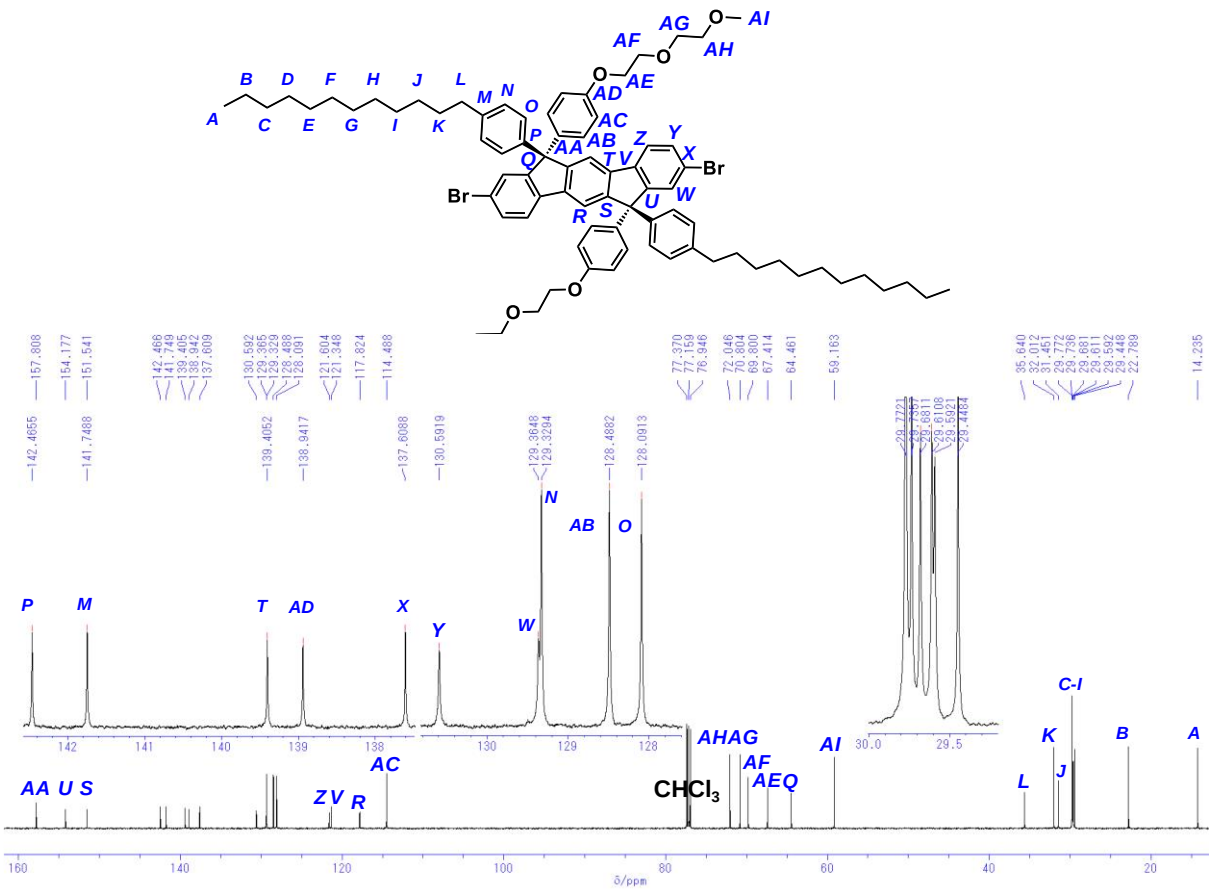

Figure S5. ^{13}C NMR spectrum of ***syn*-4** (151 MHz, $CDCl_3$ at 25 °C).

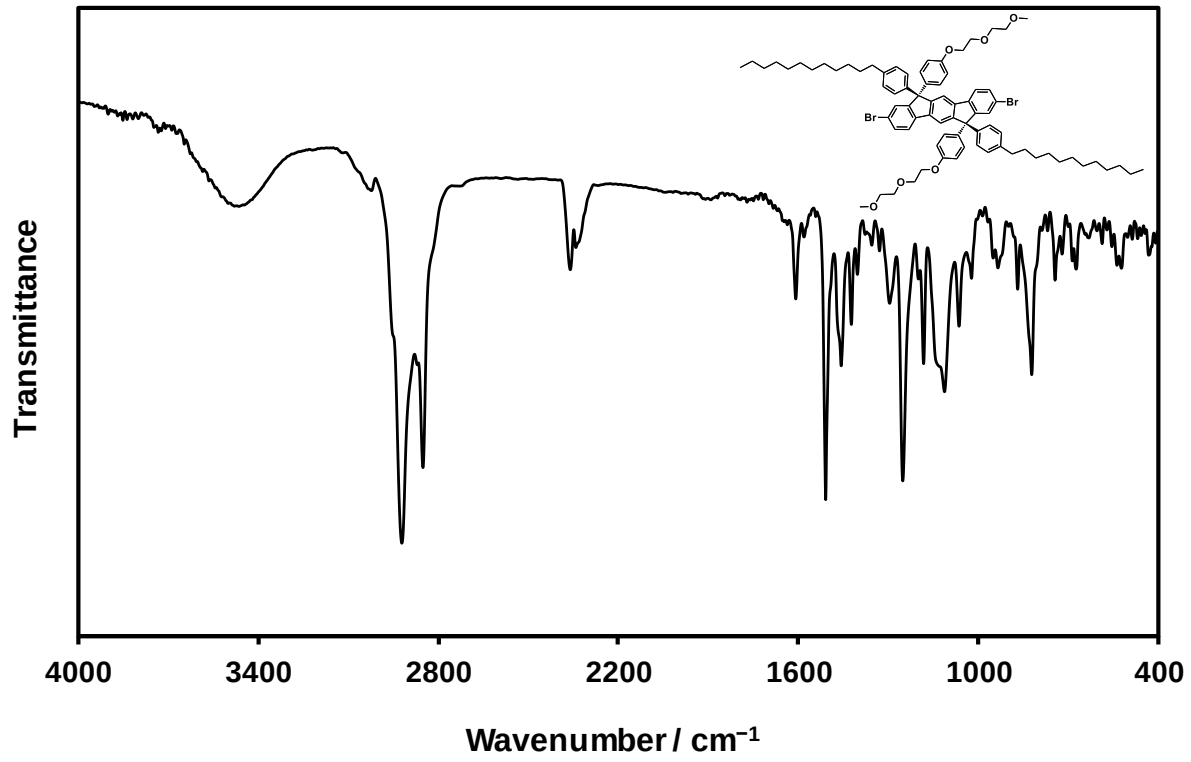

Figure S6. FT-IR spectrum of ***syn*-4** (KBr).

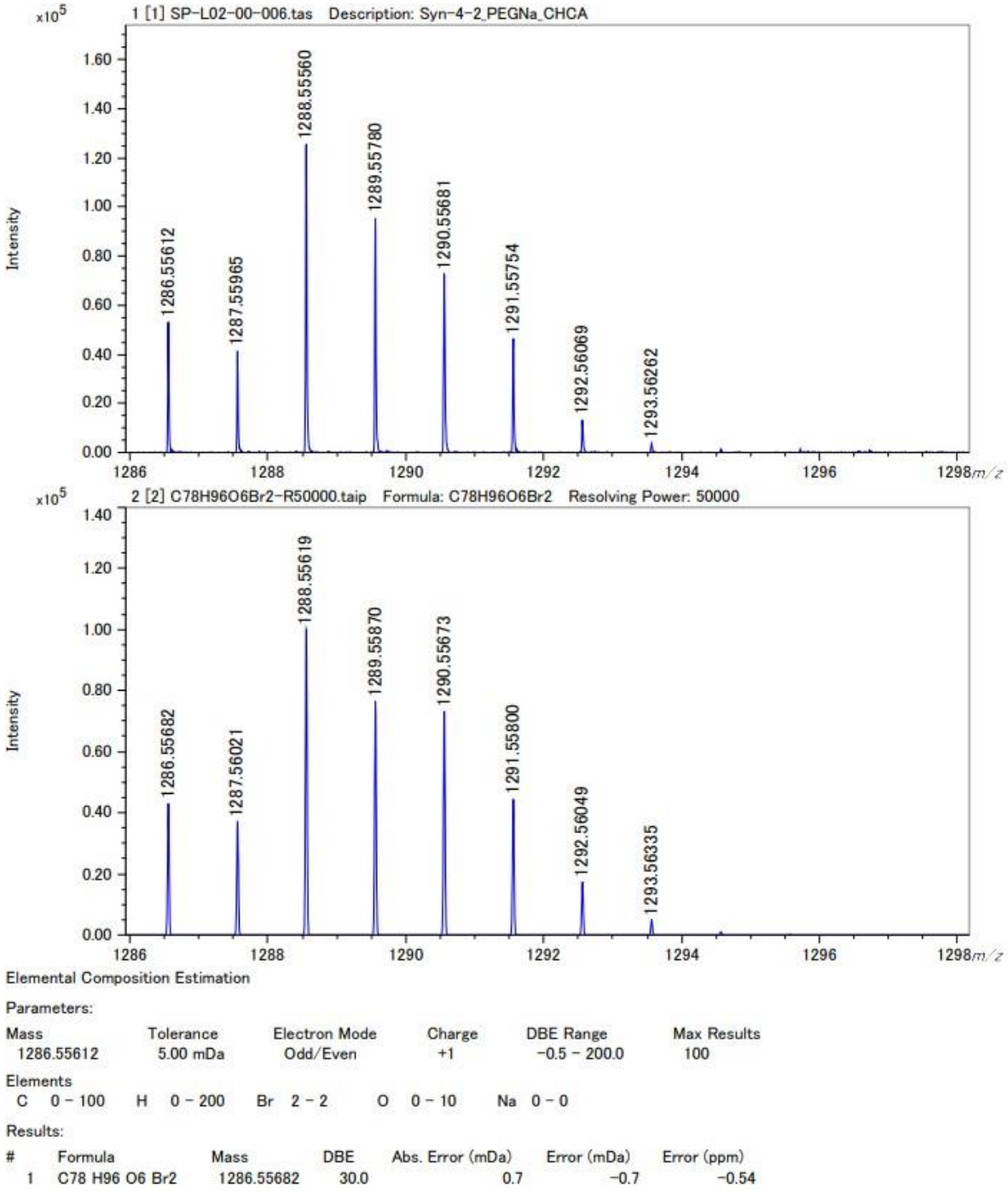

Figure S7. High-Resolution MALDI-TOF mass spectra (upper; observed, lower; simulated) of ***syn*-4**.

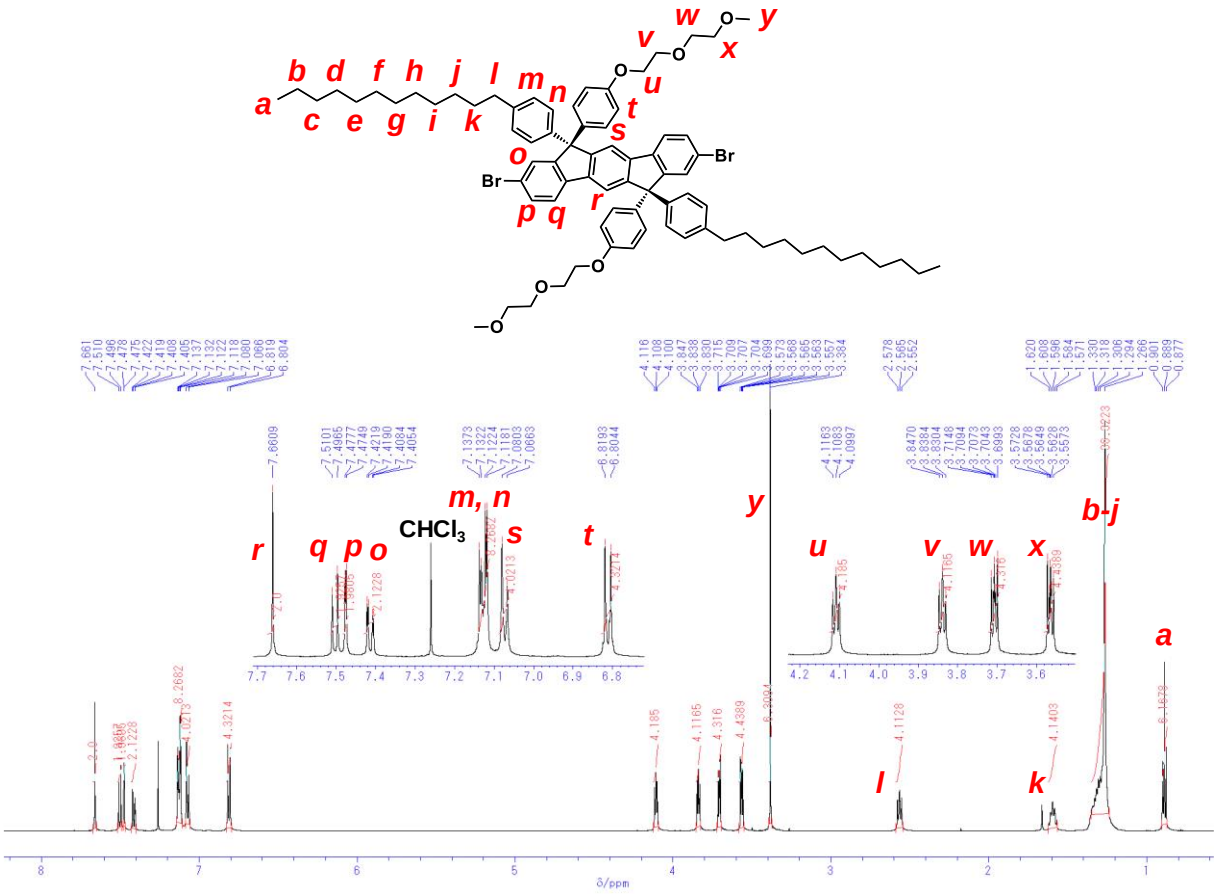

Figure S8. ^{1}H NMR spectrum of ***anti*-4** (600 MHz, $CDCl_3$ at 25 °C).

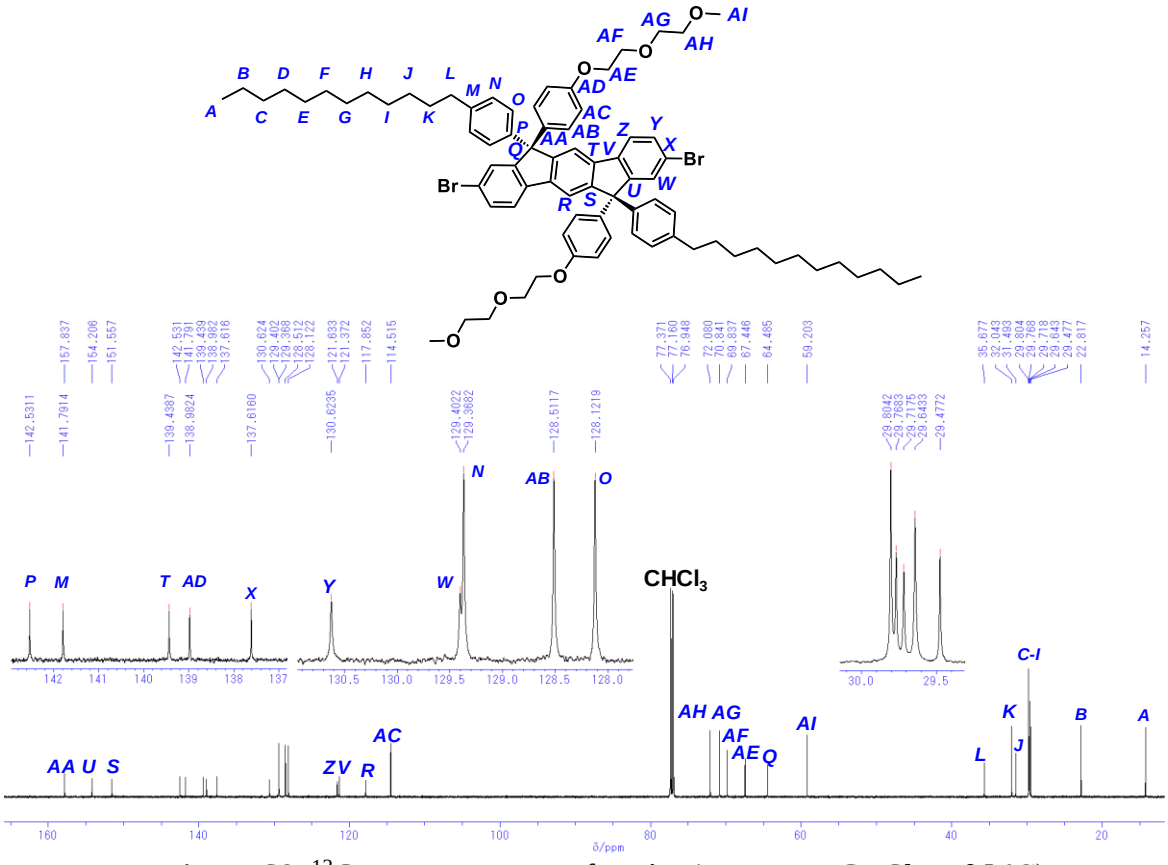

Figure S9. ^{13}C NMR spectrum of ***anti*-4** (151 MHz, $CDCl_3$ at 25 °C).

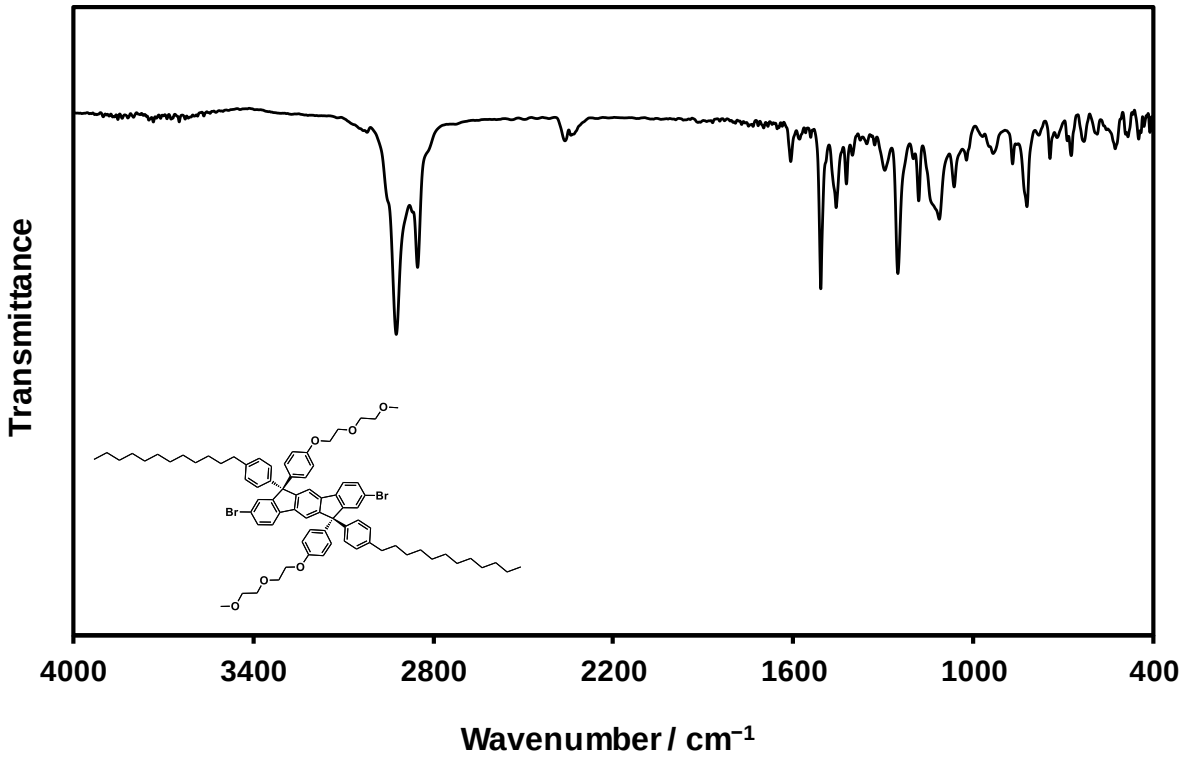

Figure S10. FT-IR spectrum of ***anti*-4** (KBr).

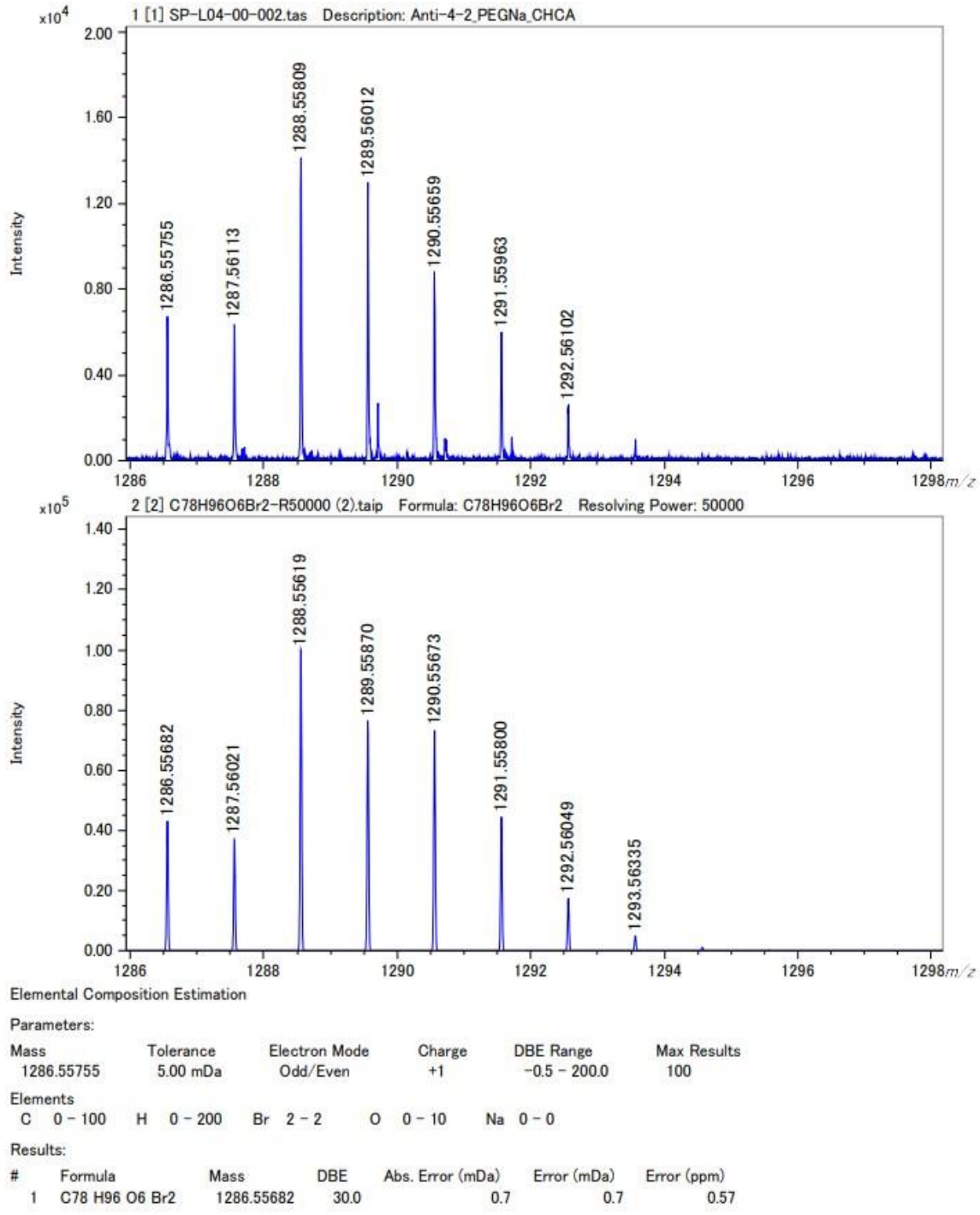

Figure S11. High-Resolution MALDI-TOF mass spectra (upper; observed, lower; simulated) of ***anti*-4**.

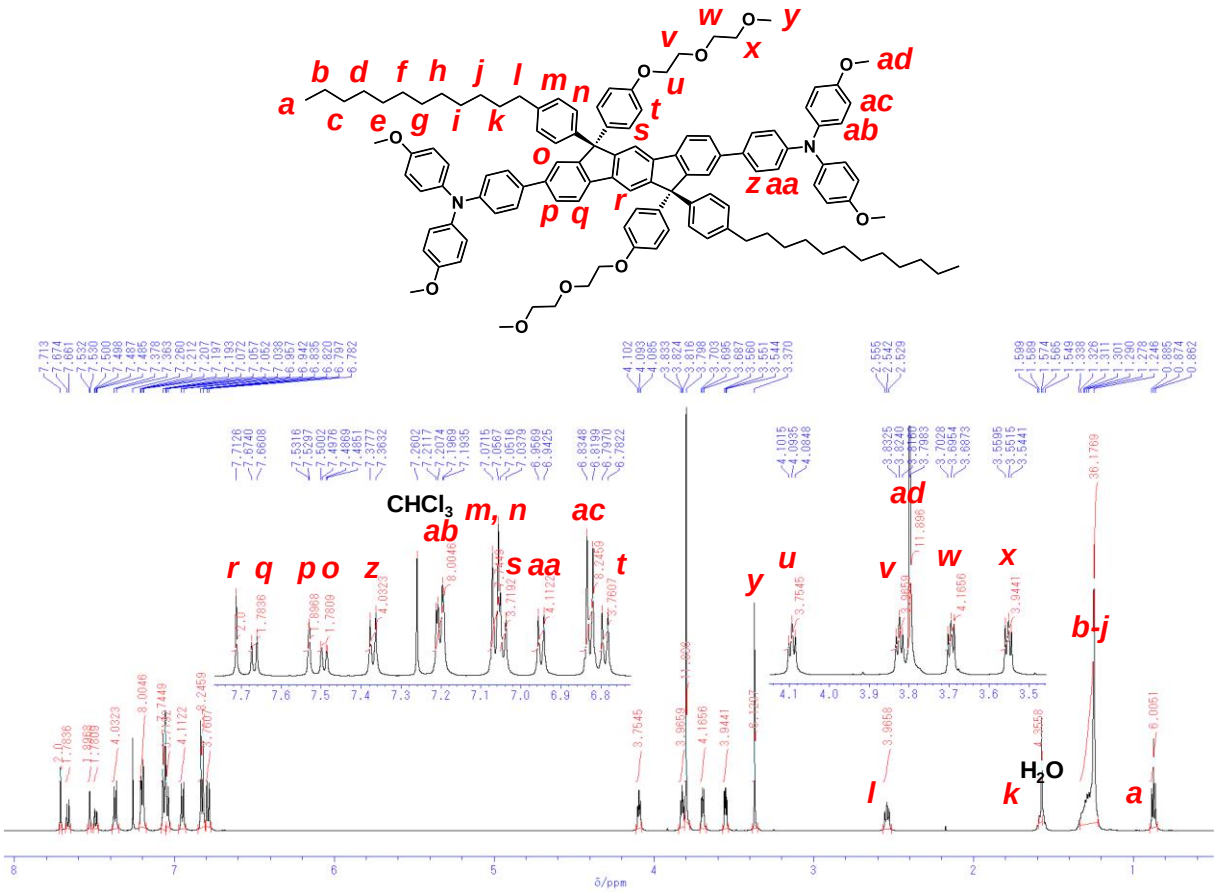

Figure S12. ^{1}H NMR spectrum of **PM-*syn*** (600 MHz, $CDCl_3$ at 25 °C).

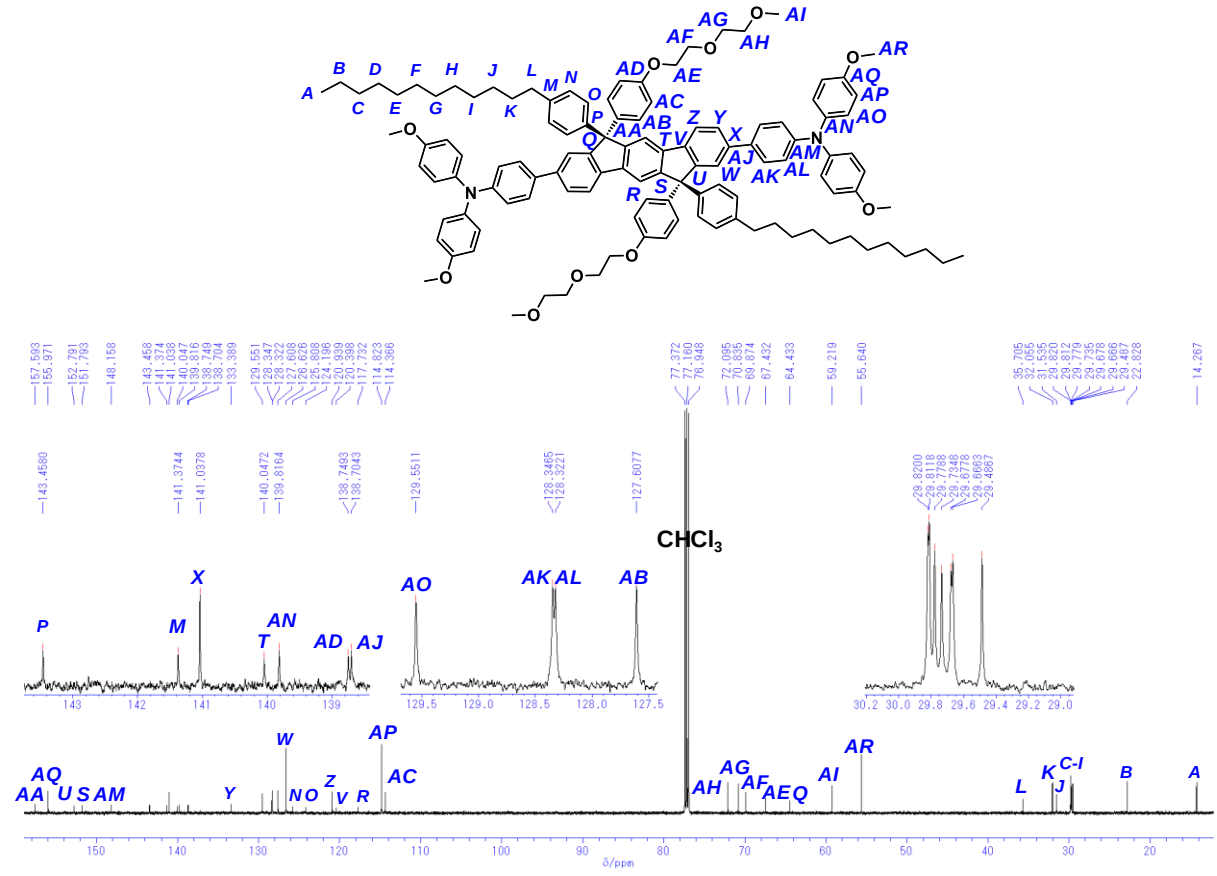

Figure S13. ^{13}C NMR spectrum of **PM-*syn*** (151 MHz, $CDCl_3$ at 25 °C).

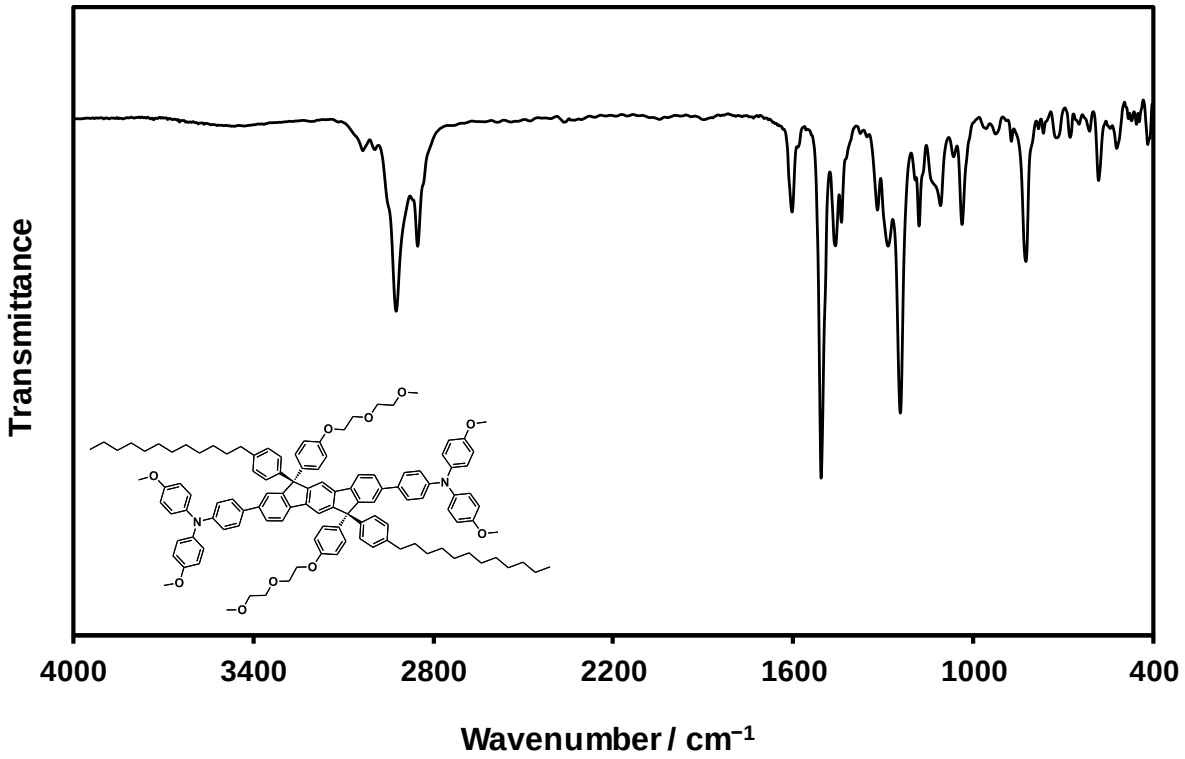

Figure S14. FT-IR spectrum of **PM-*syn*** (KBr).

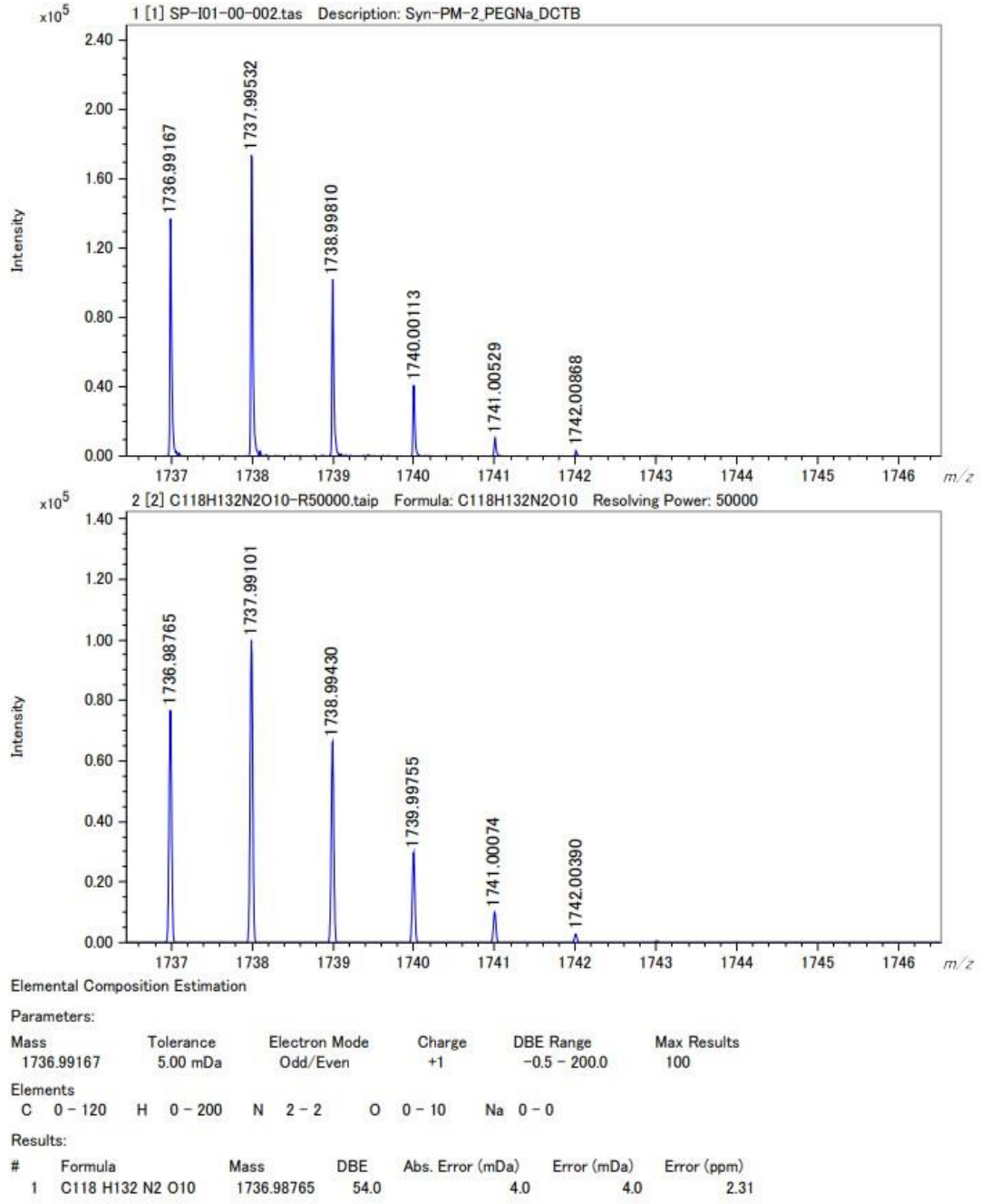

Elemental Composition Estimation

Parameters:

Mass	Tolerance	Electron Mode	Charge	DBE Range	Max Results
1736.99167	5.00 mDa	Odd/Even	+1	-0.5 - 200.0	100

Elements

C	0 - 120	H	0 - 200	N	2 - 2	O	0 - 10	Na	0 - 0

Results:

#	Formula	Mass	DBE	Abs. Error (mDa)	Error (mDa)	Error (ppm)
1	C118 H132 N2 O10	1736.98765	54.0	4.0	4.0	2.31

Figure S15. High-Resolution MALDI-TOF mass spectra (upper; observed, lower; simulated) of **PM-*syn***.

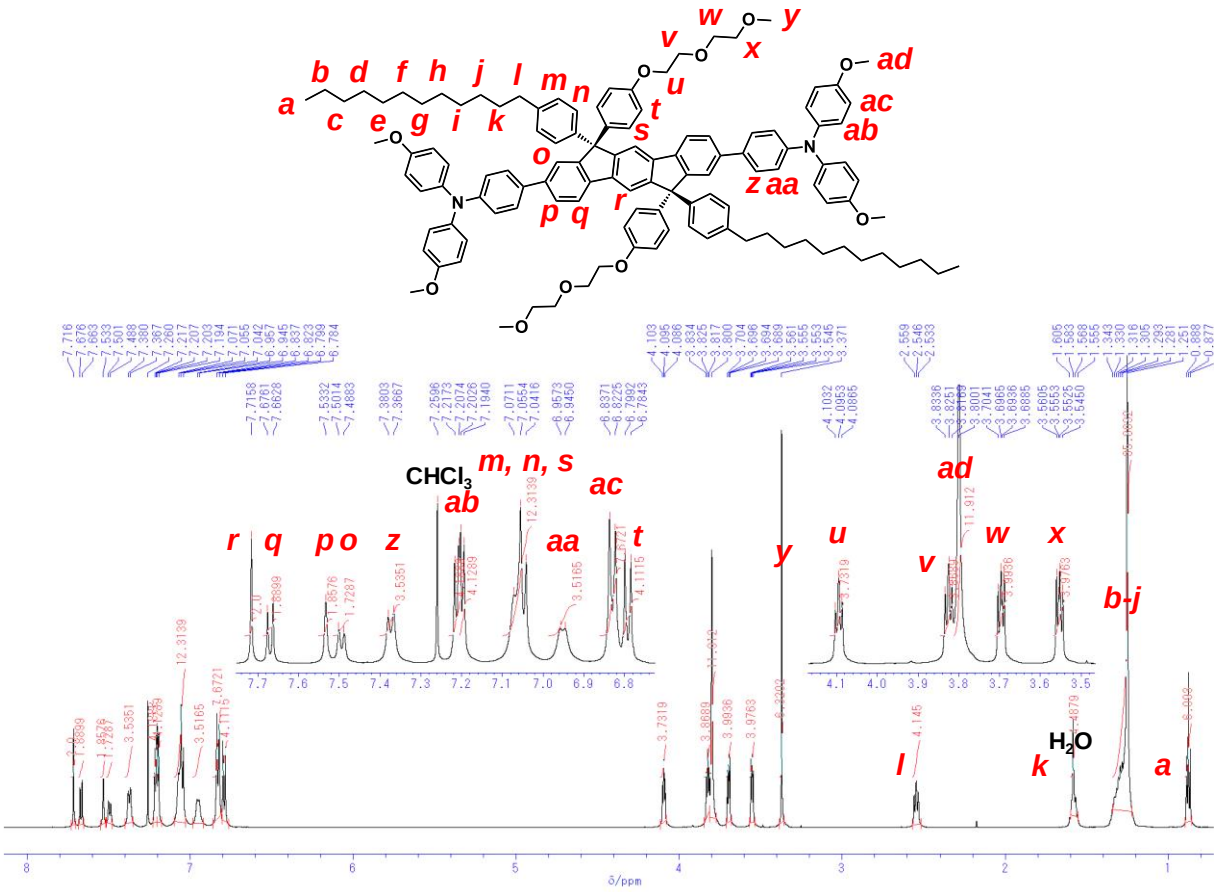

Figure S16. ^{1}H NMR spectrum of **PM-*anti*** (600 MHz, $CDCl_3$ at 25 °C).

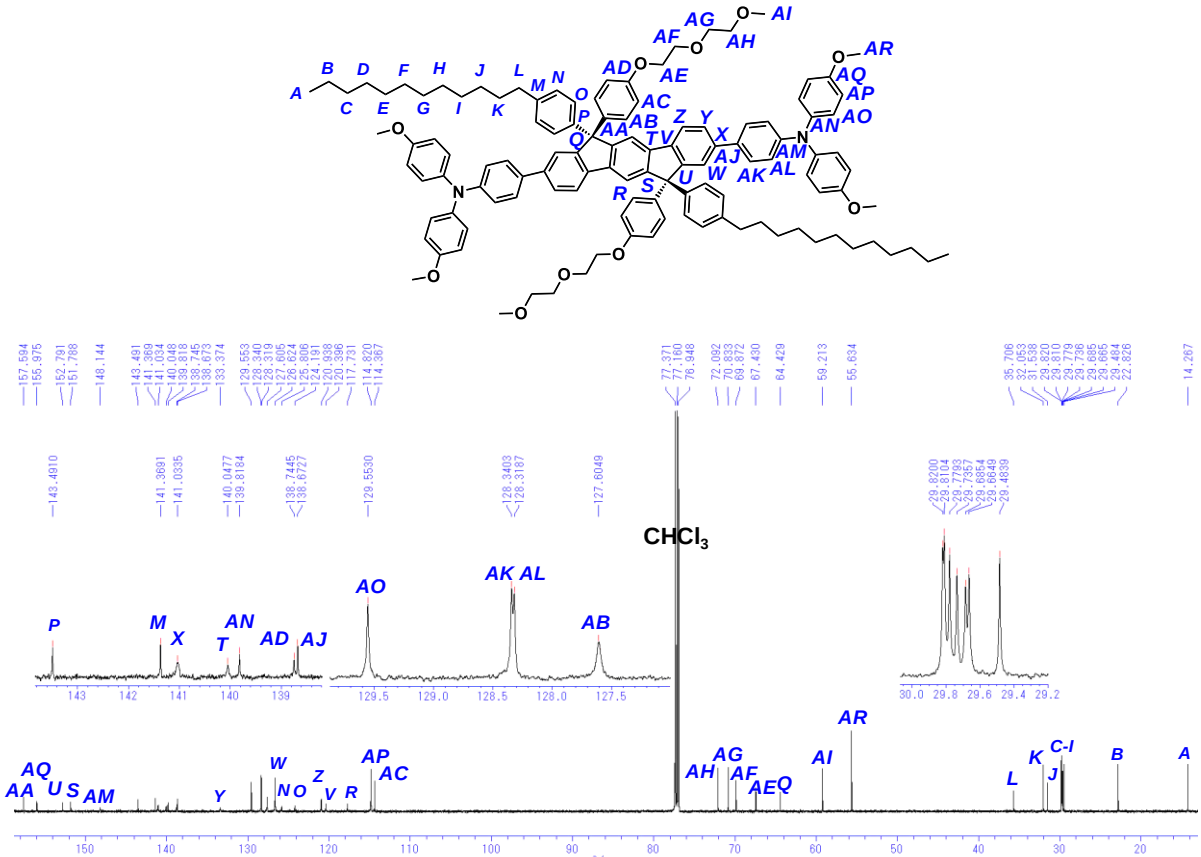

Figure S17. ^{13}C NMR spectrum of **PM-*anti*** (151 MHz, $CDCl_3$ at 25 °C).

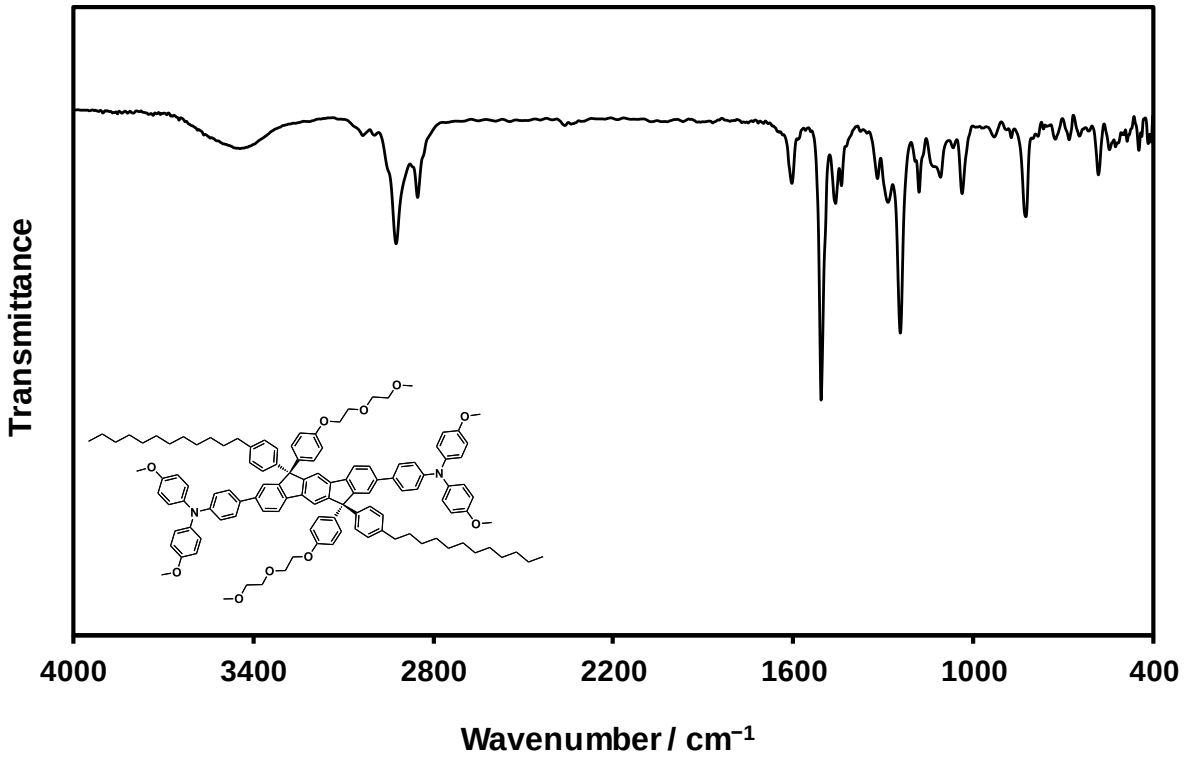

Figure S18. FT-IR spectrum of **PM-*anti*** (KBr).

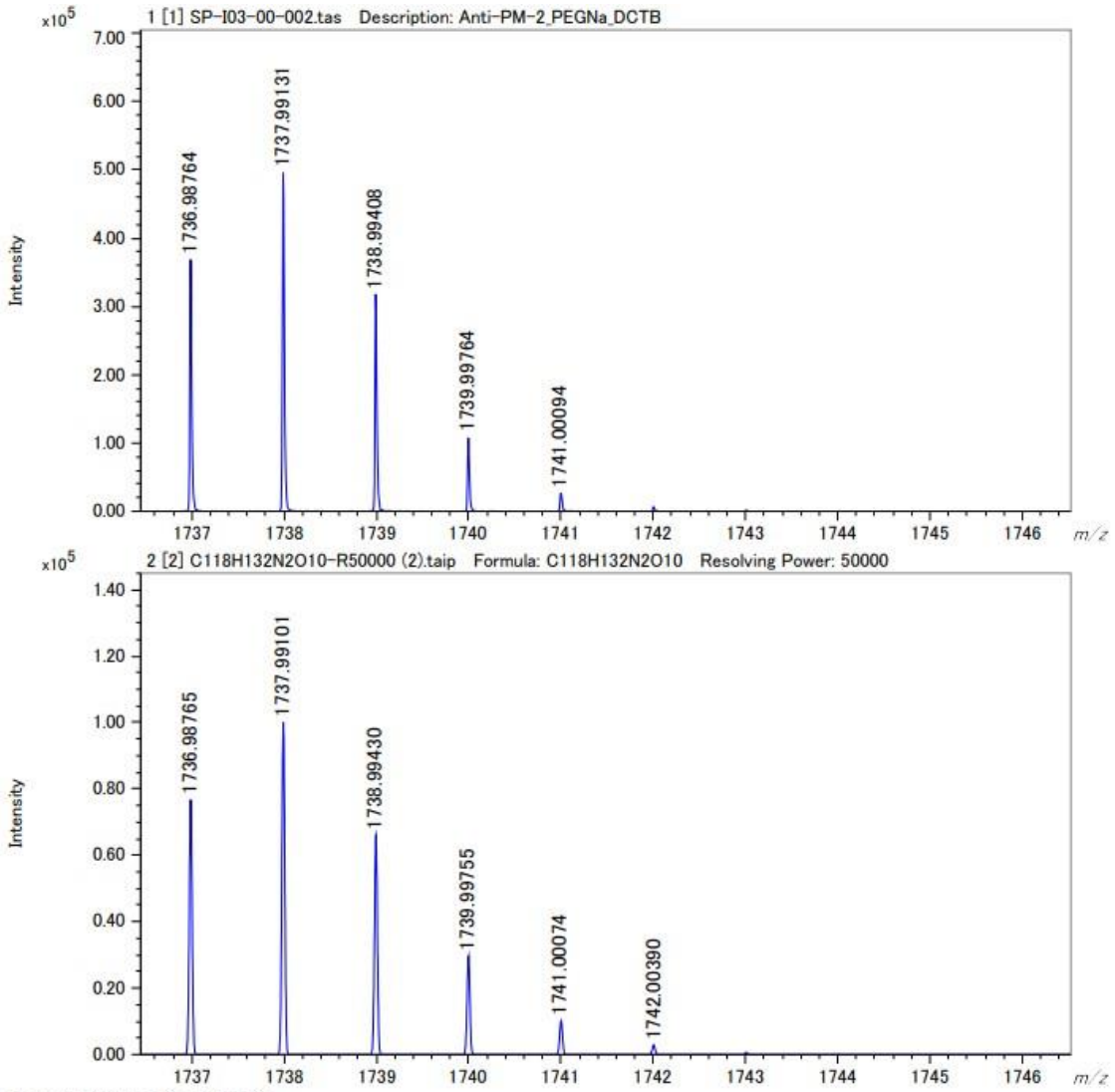

Elemental Composition Estimation

Parameters:

Mass	Tolerance	Electron Mode	Charge	DBE Range	Max Results
1736.98764	5.00 mDa	Odd/Even	+1	-0.5 - 200.0	100

Elements

C 0 - 120 H 0 - 200 N 2 - 2 O 0 - 10 Na 0 - 0

Results:

#	Formula	Mass	DBE	Abs. Error (mDa)	Error (mDa)	Error (ppm)
1	C118 H132 N2 O10	1736.98765	54.0	0.0	0.0	-0.01

Figure S19. High-Resolution MALDI-TOF mass spectra (upper; observed, lower; simulated) of **PM-*anti***.

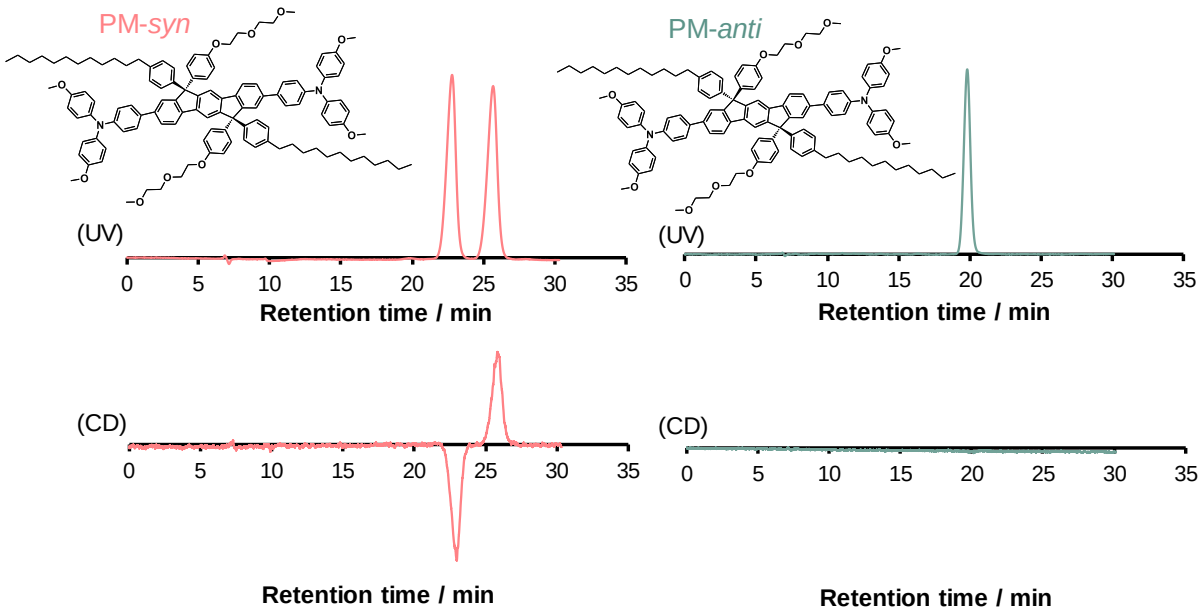

Figure S20. Chiral column charts of **PM-*syn*** and **PM-*anti***. The top and bottom charts are ultraviolet (UV) absorption and circular dichroism (CD) data, respectively. In the HPLC chart of **PM-*syn***, two peaks with the same peak area and opposite CD sign were observed, indicating the chiral resolution of **PM-*syn***. On the other hand, only one peak with no CD signal was observed for **PM-*anti***. These observation indicate **PM-*syn*** is a chiral species with bifacial structure, and **PM-*anti*** is an achiral and non-bifacial *meso* species.

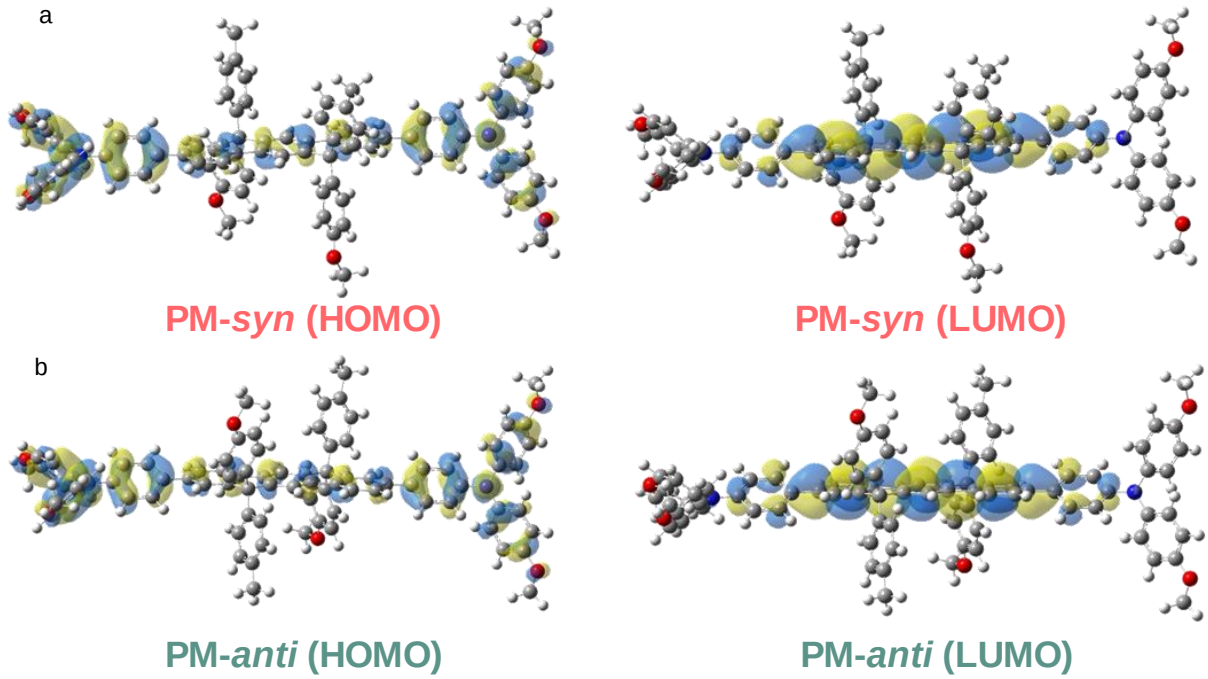

Figure S21. HOMO (left) and LUMO (right) lobes calculated by DFT for (a) PM-*syn* and (b) PM-*anti*. For simplicity, DEG and *n*-dodecyl are replaced by methoxy and methyl, respectively.

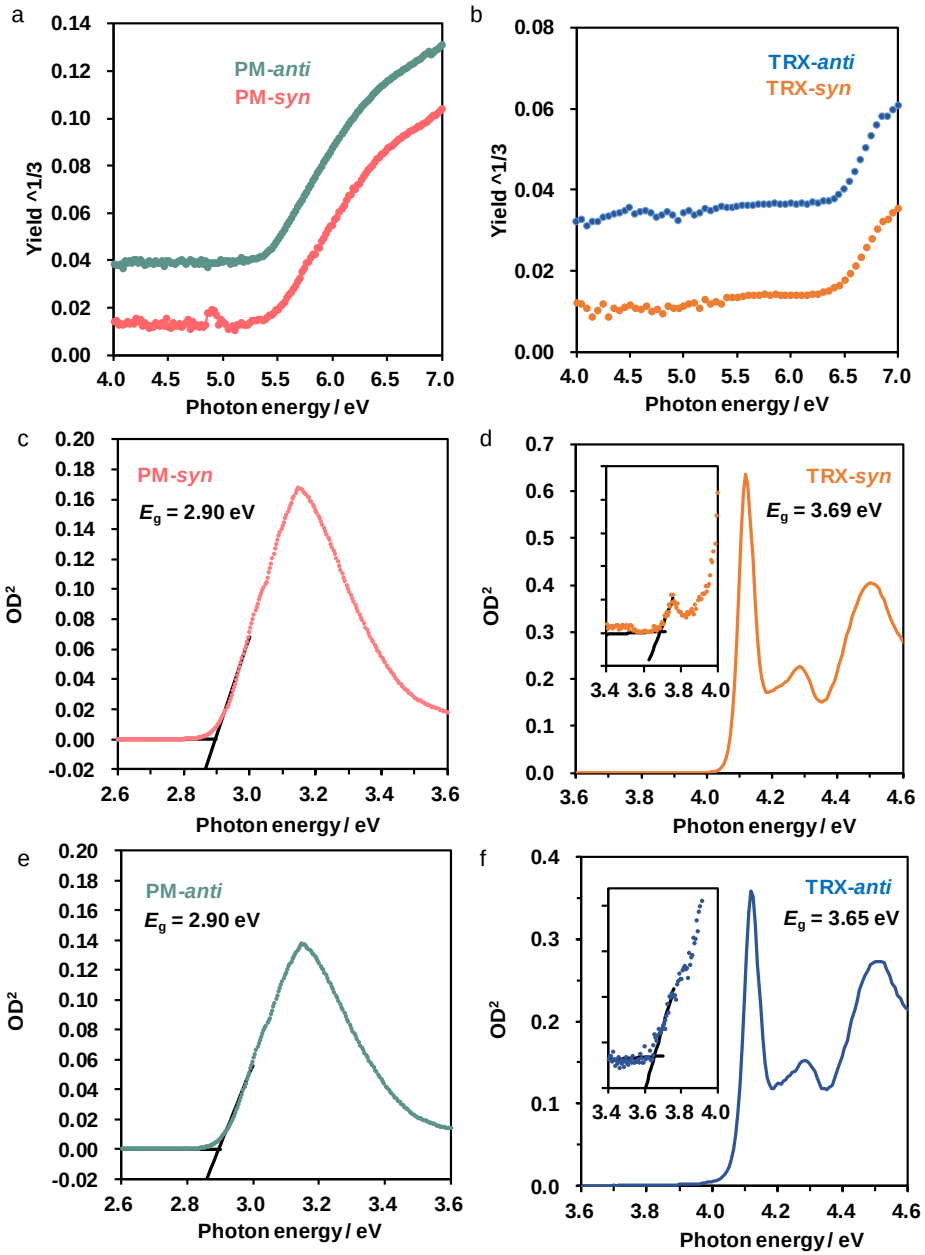

Figure S22. Photoelectron yield spectra of (a) PM-*syn* and PM-*anti* and (b) TRX-*syn* and TRX-*anti* measured by PYS. Photoabsorption edge of solutions (chloroform for PM and THF for TRX) to calculate the optical bandgap for (c) PM-*syn*, (d) PM-*anti*, (e) TRX-*syn*, and (f) TRX-*anti*. Since the bandedge of TRX is attributed to forbitten transition, the magnified plots are shown in the inset.

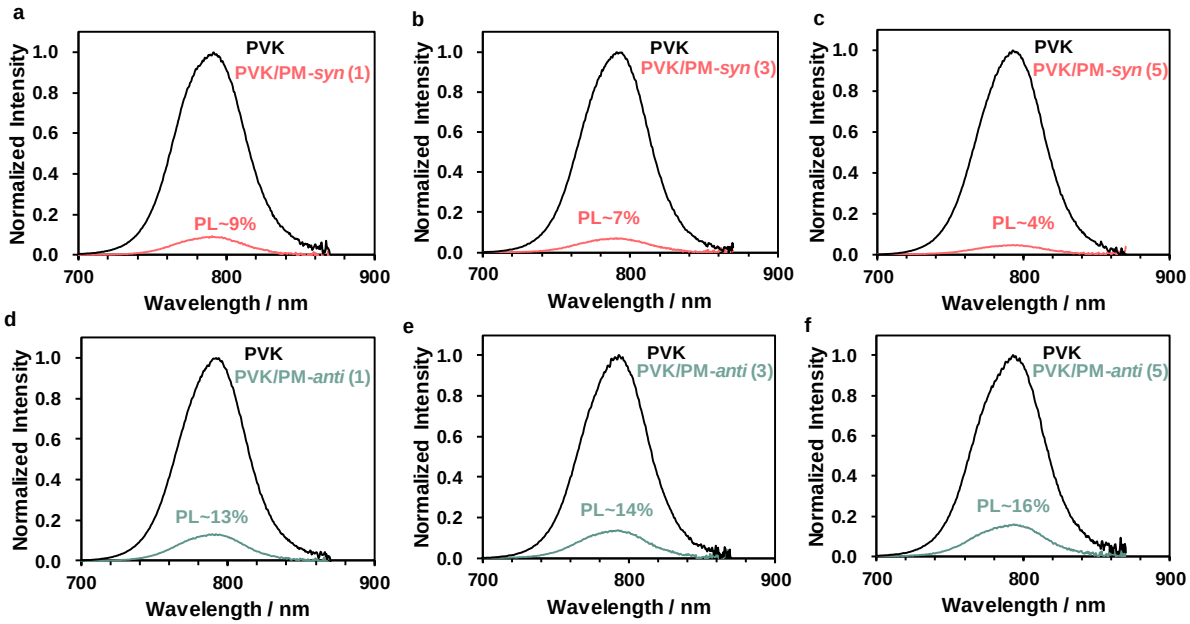

Figure S23. PL spectra of PVK with/without (a)-(c) PM-*syn* and (d)-(f) PM-*anti* passivation (λ_{ex} = 500 nm). The values in the brackets indicate the concentration of PM in CB (mg mL^{-1}).

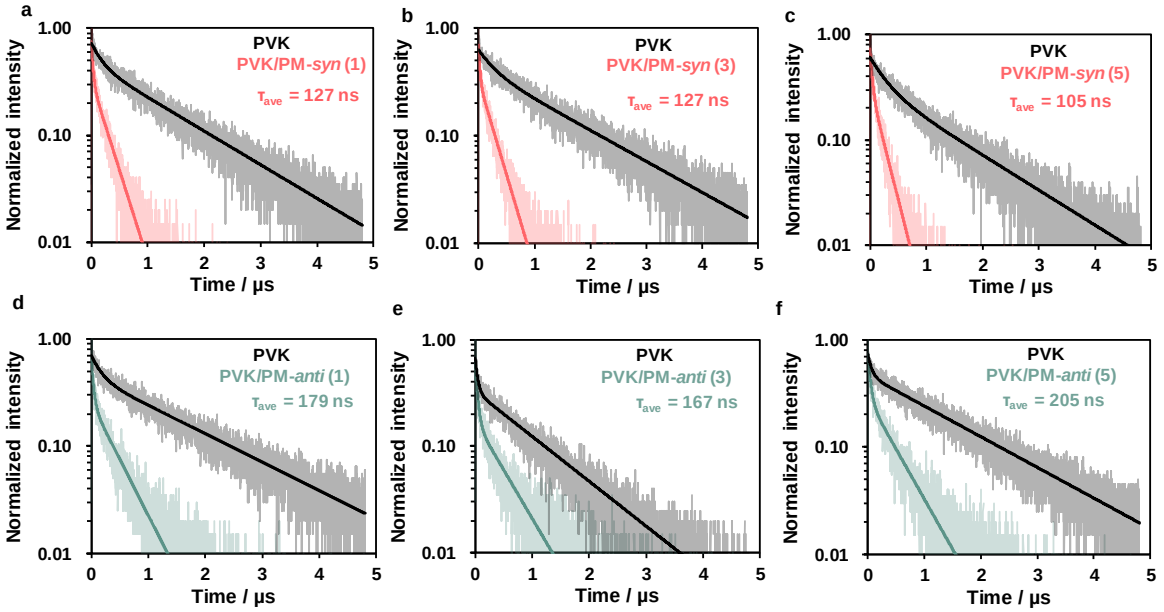

Figure S24. TRPL decays of PVK with/without (a)-(c) PM-*syn* and (d)-(f) PM-*anti* passivation (λ_{ex} = 377 nm, λ_{em} = 770 nm). The values in the brackets indicate the concentration of PM in CB (mg mL^{-1}). The averaged lifetimes (τ_{ave}, **Table S1**) are imposed.

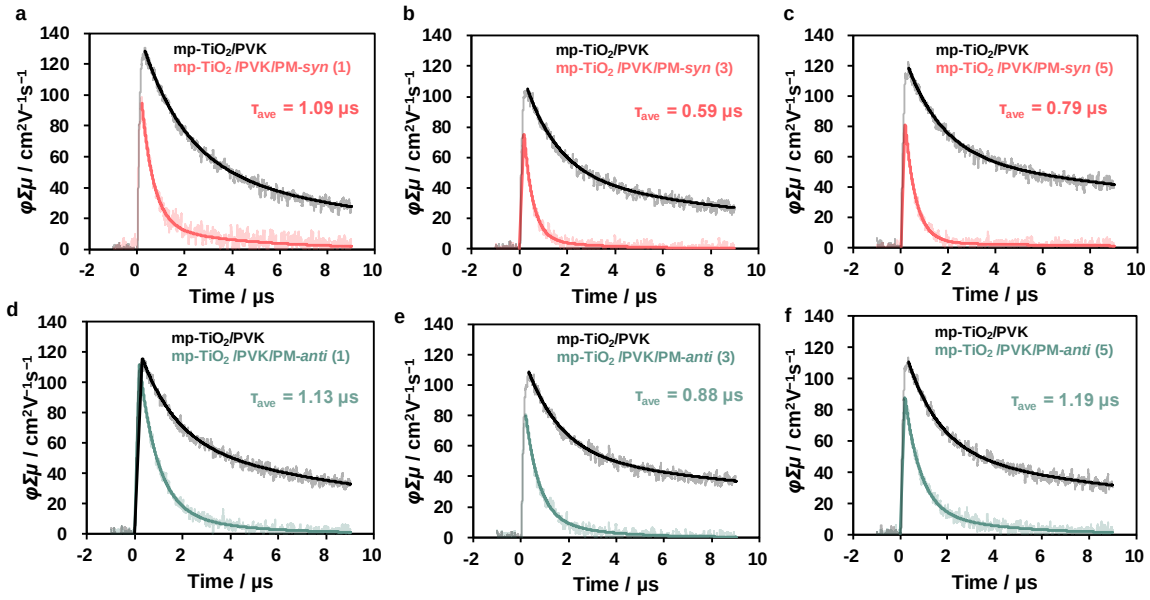

Figure S25. TRMC decays of PVK with/without (a)-(c) PM-*syn* and (d)-(f) PM-*anti* passivation (λ_{ex} = 500 nm). The values in the brackets indicate the concentration of PM in CB (mg mL^{-1}). The averaged lifetimes (τ_{ave}, **Table S2**) are imposed.

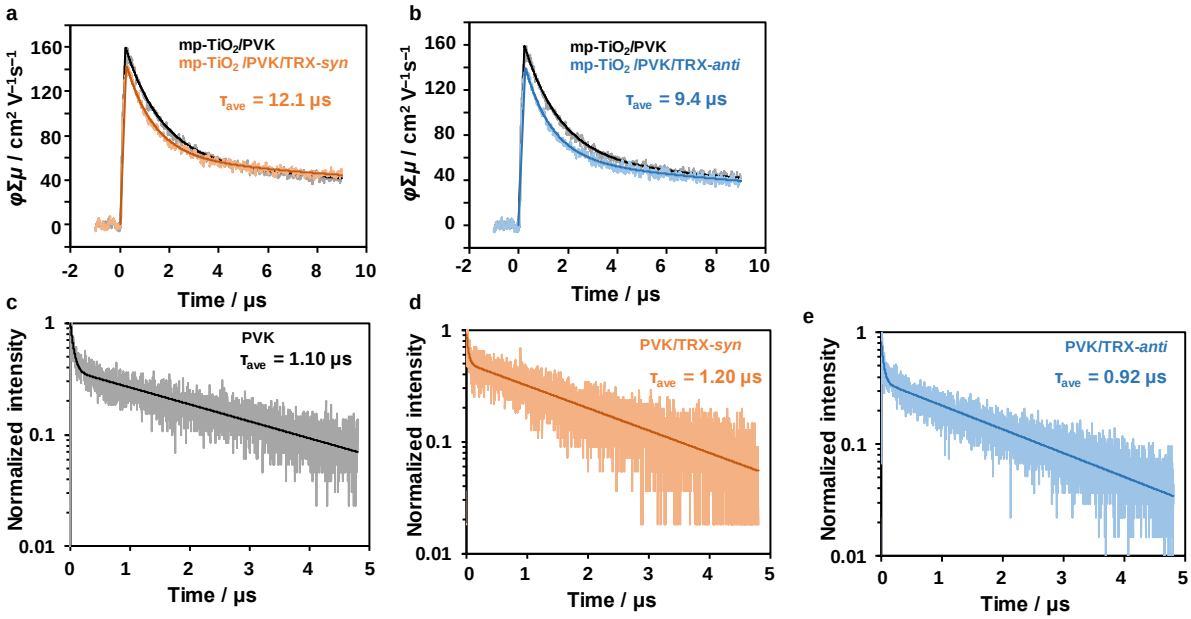

Figure S26. TRMC decays of PVK on mpTiO$_2$ with/without (a) TRX-*syn* and (b) TRX-*anti* passivation (λ_{ex} = 500 nm). The averaged lifetimes (τ_{ave}, **Table S2**) are imposed. TRPL decays of (c) PVK, (d) TRX-*syn*-treated PVK, and (e) TRX-*anti*-treated PVK. λ_{ex} = 377 nm, λ_{em} = 770 nm. The averaged lifetimes (τ_{ave}, **Table S1**) are imposed. The concentration of TRX was 0.5 mg mL^{-1} in isopropylalcohol.

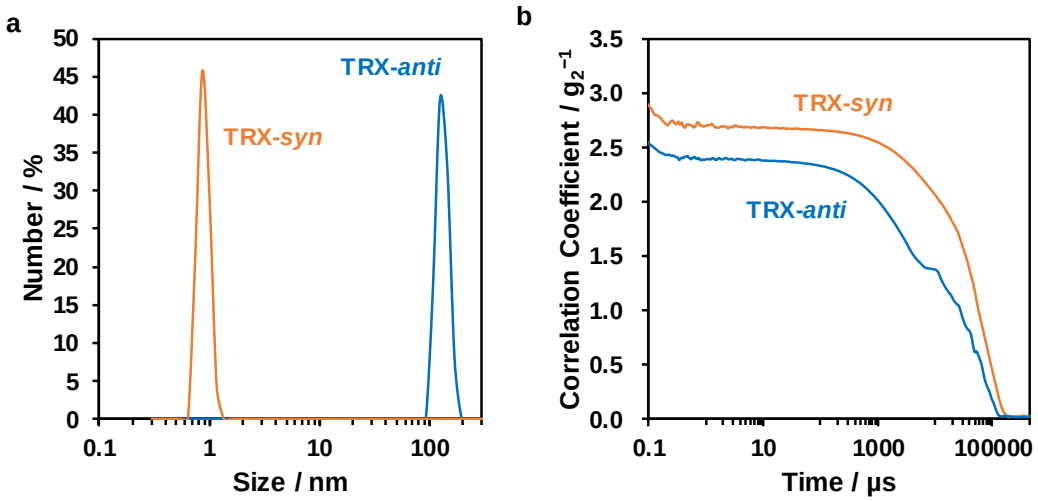

Figure S27. (a) DLS particle size distribution of TRX-*syn* and TRX-*anti* in IPA (0.5 mg mL^{-1}). (b) Autocorrelation function decays.

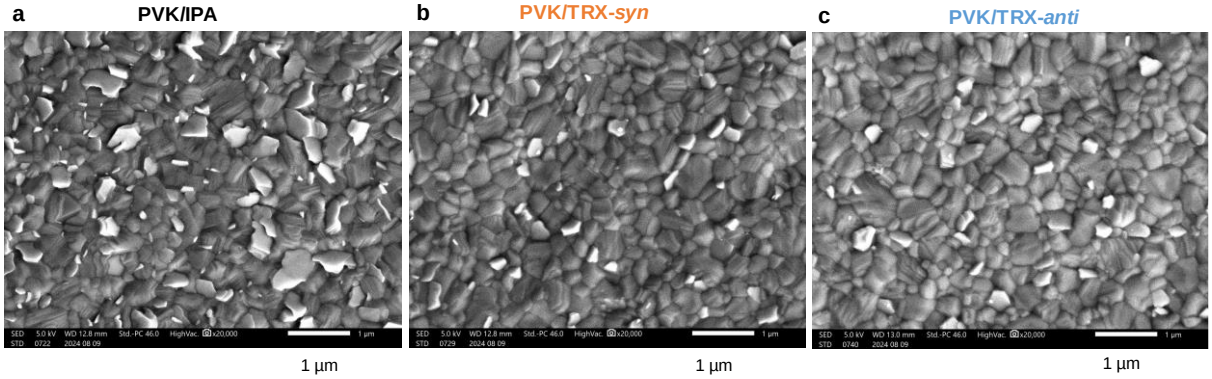

Figure S28 SEM images of (a) PVK, (b) PVK after TRX-*syn* passivation, and (c) PVK after TRX-*anti* passivation. The scale bar is 1 µm.

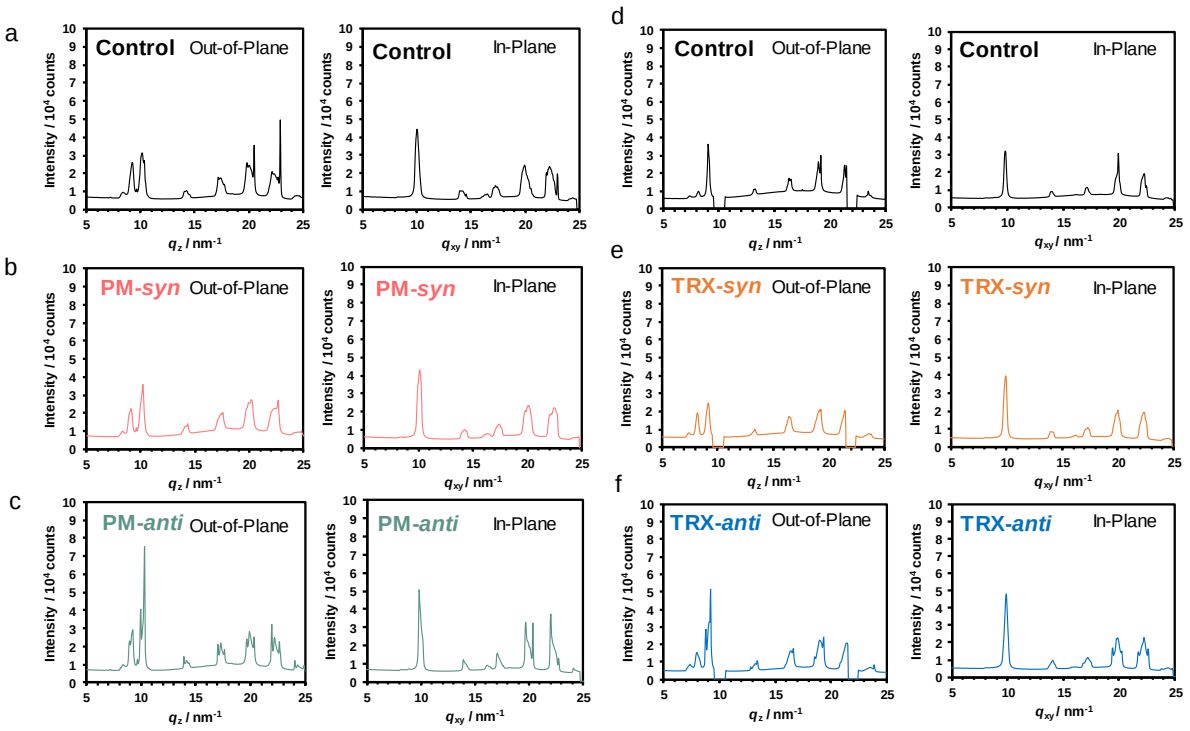

Figure S29. 2D-GIXRD profiles of (a)-(c) PVK with/without PM-*syn* or PM-*anti* passivation and (d)-(f) PVK with/without TRX-*syn* or TRX-*anti* passivation. The left and right panels for each are the out-of-plane and in-plane profiles, respectively. λ = 1 Å.

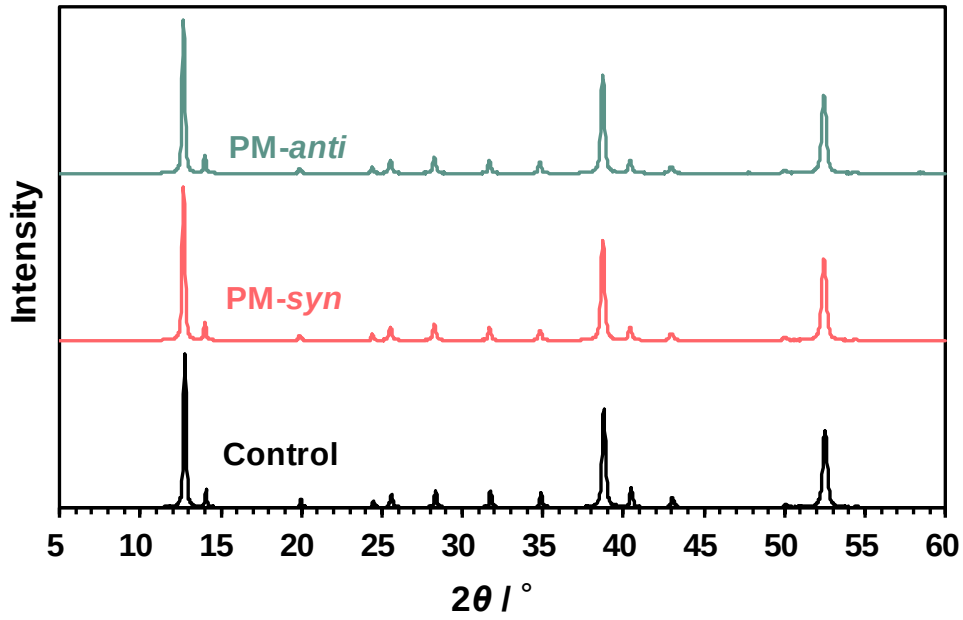

Figure S30. Power XRD profiles of PVK with/without PM-*syn* or PM-*anti* passivation. λ = 1.54 Å.

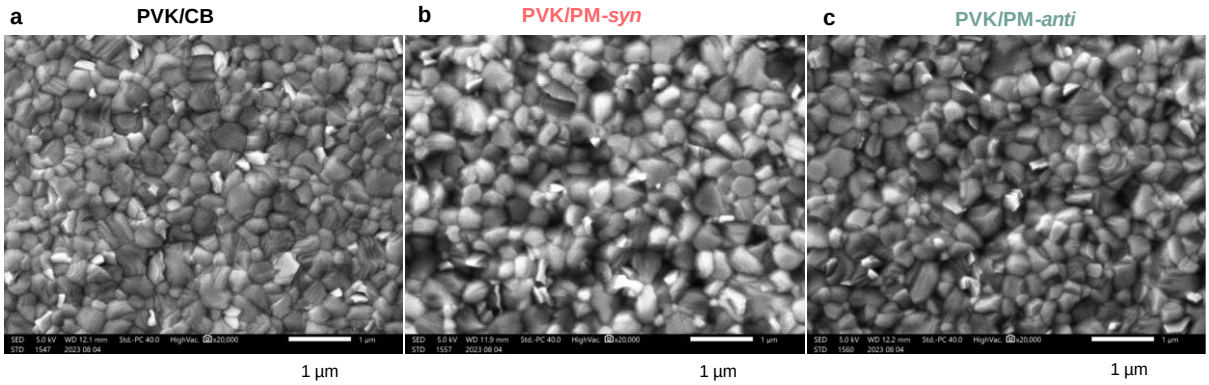

Figure S31. SEM images of (a) PVK, (b) PVK after PM-*syn* passivation, and (c) PVK after PM-*anti* passivation. The scale bar is 1 µm.

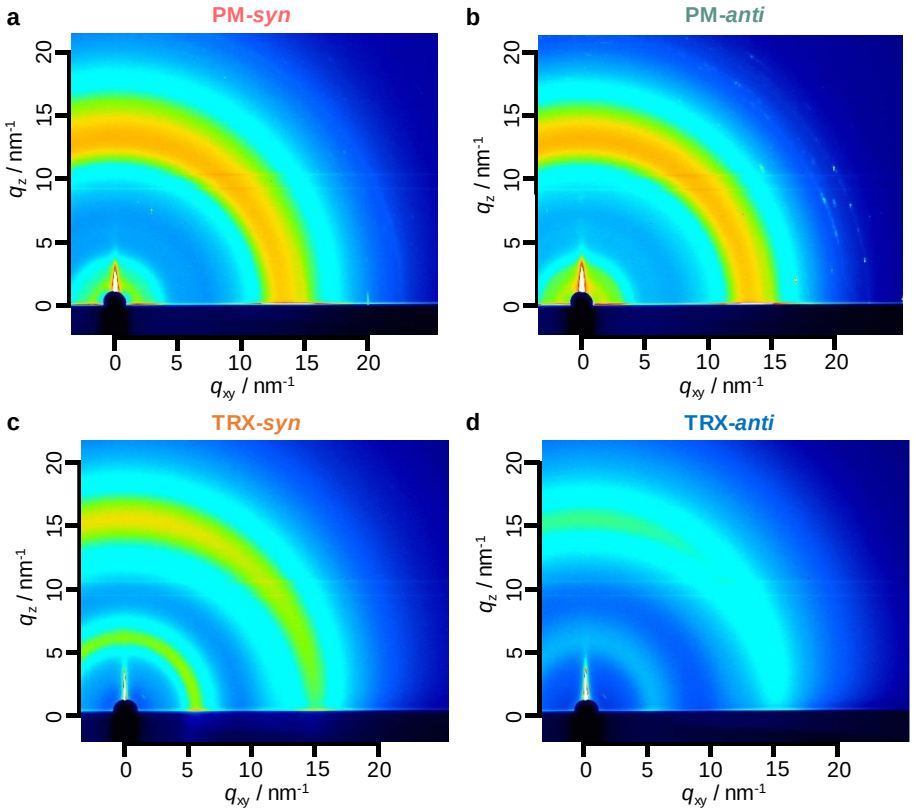

Figure S32. 2D-GIXRD images of (a) PM-*syn*, (b) PM-*anti*, (c) TRX-*syn*, and (d) TRX-*anti* films. λ = 1 Å.

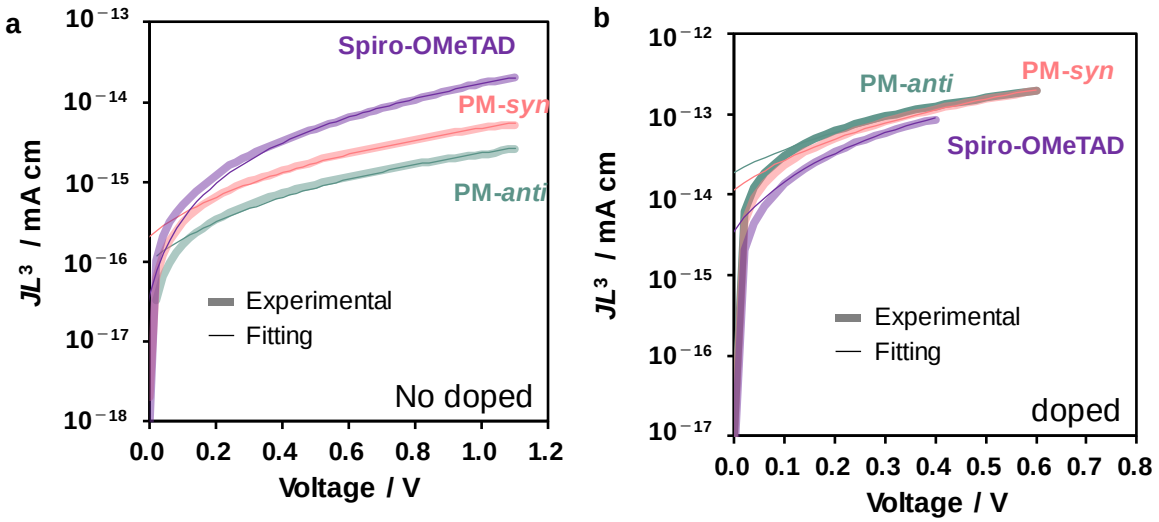

Figure S33. SCLC curves of spiro-OMeTAD, PM-*syn*, and PM-*anti* in hole-only devices (ITO/PEDOT:PSS/molecules/Au). (b) Those with dopants (LiTFSI).

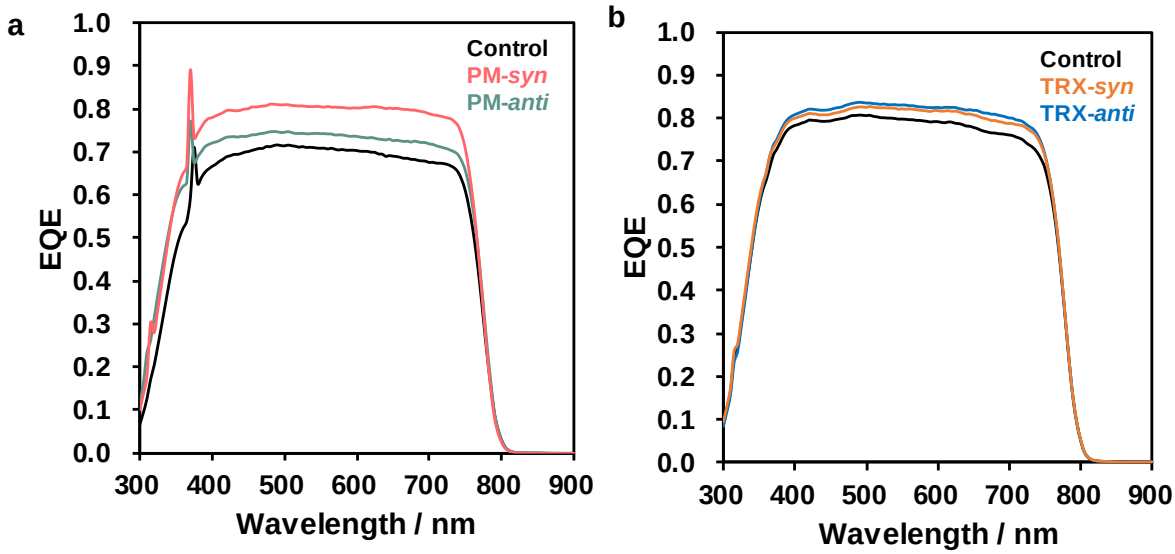

Figure S34. EQE spectra of (a) PVK with/without PM-*syn* or PM-*anti* passivation and PVK with/without TRX-*syn* or TRX-*anti* passivation. The spikes in (a) are artifacts caused by a filter change. The integrated J_{SC} values were (a) 17.3 (control), 19.9 (PM-*syn*), 18.4 (PM-*anti*), (b) 20.4 (control), 20.3 (TRX-*syn*), 20.6 (TRX-*anti*) mA cm^{-2}. They are smaller than the J_{SC} under pseudo sunlight, probably due to the degradation and/or low light intensity in the EQE measurements. The issue of J_{SC} mismatch can be seen in a reference.[S4]

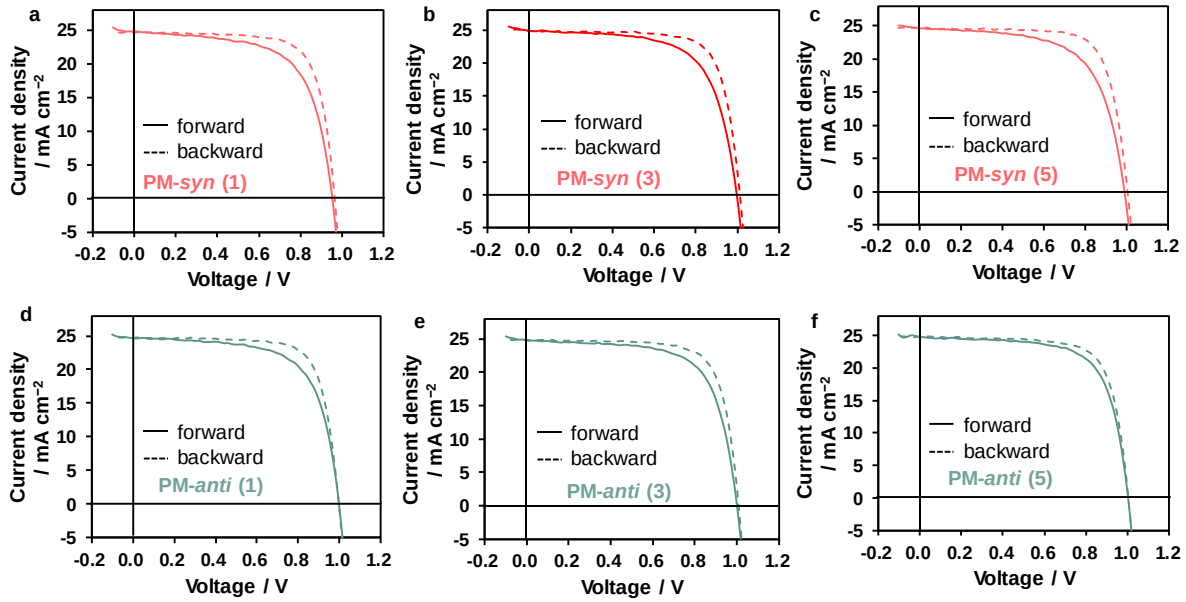

Figure S35. *J–V* curves of PSCs at different concentrations of (a)-(c) PM-*syn* and (d)-(f) PM-*anti* passivation. The values in the bracket show the concentration (mg mL^{-1}). The solid and dotted lines are forward and reverse (backward) scans, respectively.

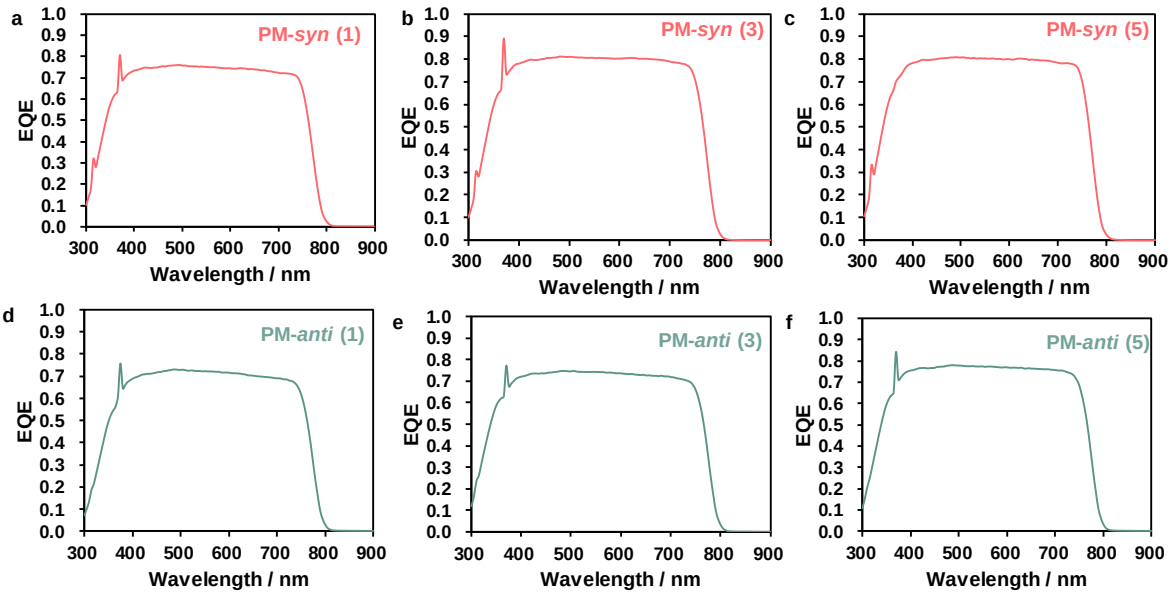

Figure S36. EQE spectra of PSCs at different concentrations of (a)-(c) PM-*syn* and (d)-(f) PM-*anti* passivation. The values in the bracket show the concentration (mg mL^{-1}). The spikes are artifacts caused by a filter change.

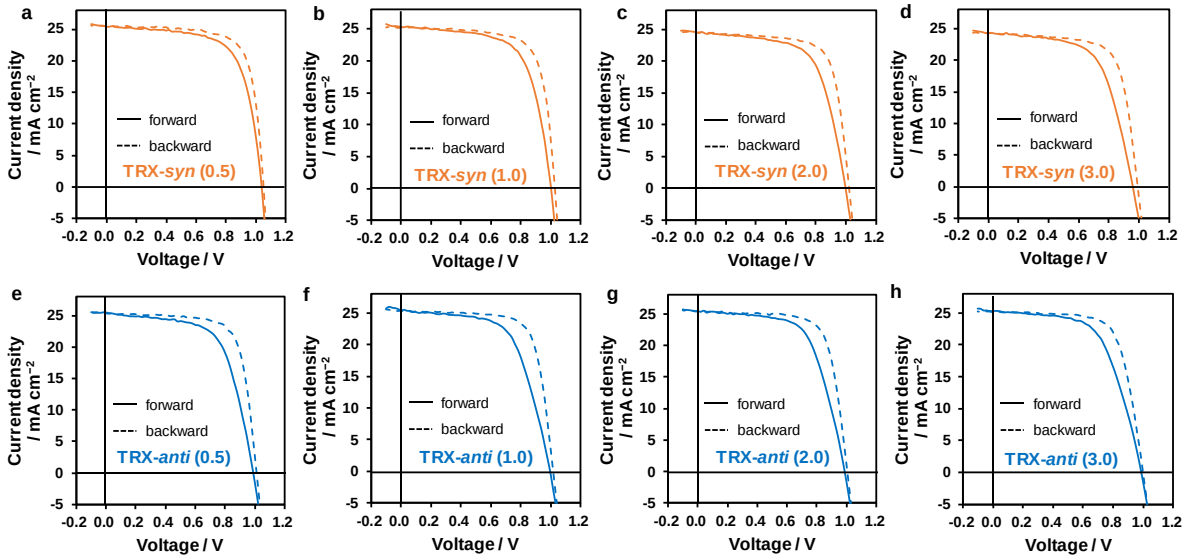

Figure S37. *J–V* curves of PSCs at different concentrations of (a)-(d) TRX-*syn* and (e)-(h) TRX-*anti* passivation. The values in the bracket show the concentration (mg mL^{-1}). The solid and dotted lines are forward and reverse (backward) scans, respectively.

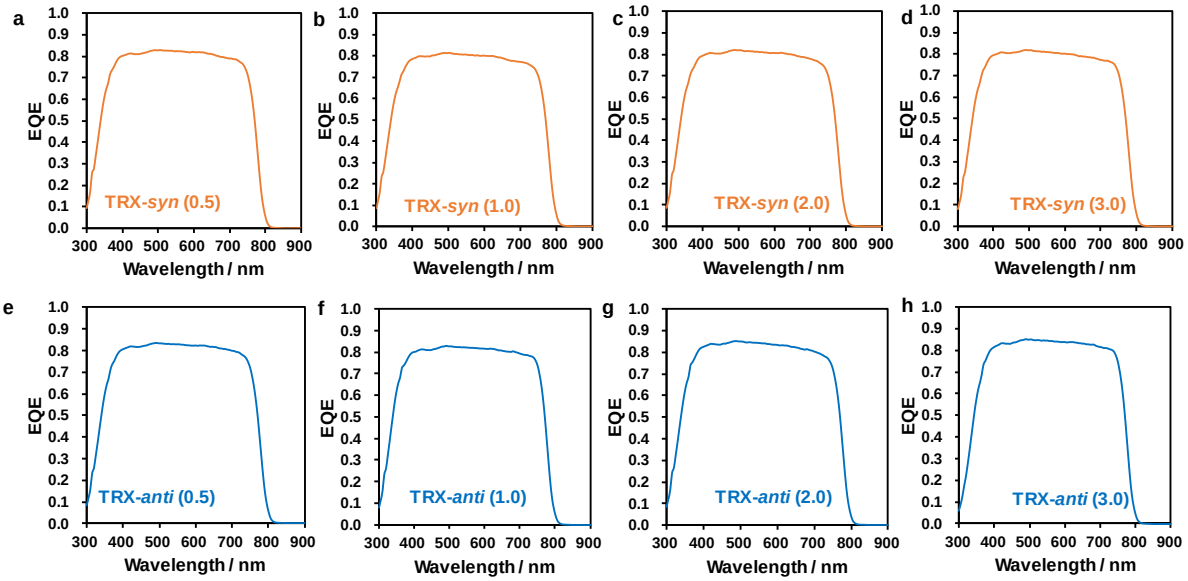

Figure S38. EQE spectra of PSCs at different concentrations of (a)-(d) TRX-*syn* and (e)-(h) TRX-*anti* passivation. The values in the bracket show the concentration (mg mL^{-1}). The spikes are artifacts caused by a filter change.

Supporting reference

(S1) T. Omine, F. Ishiwari, T. Won, N. Aizawa, Y. Takeda, Y. Yakiyama, T. Mori, T. Hirose, K.-i. Nakayama and A. Saeki, *ChemRxiv*, DOI: 10.26434/chemrxiv-2024-m8drx.

(S2) N. Minoi, F. Ishiwari, K. Murotani, R. Nishikubo, T. Fukushima and A. Saeki, *ACS Appl. Mater. Interfaces*, 2023, **15**, 6708–6715.

(S3) M. J. Frisch, G. W. Trucks, H. B. Schlegel, G. E. Scuseria, M. A. Robb, J. R. Cheeseman, G. Scalmani, V. Barone, G. A. Petersson, H. Nakatsuji, X. Li, M. Caricato, A. V. Marenich, J. Bloino, B. G. Janesko, R. Gomperts, B. Mennucci, H. P. Hratchian, J. V. Ortiz, A. F. Izmaylov, J. L. Sonnenberg, D. Williams-Young, F. Ding, F. Lipparini, F. Egidi, J. Goings, B. Peng, A. Petrone, T. Henderson, D. Ranasinghe, V. G. Zakrzewski, J. Gao, N. Rega, G. Zheng, W. Liang, M. Hada, M. Ehara, K. Toyota, R. Fukuda, J. Hasegawa, M. Ishida, T. Nakajima, Y. Honda, O. Kitao, H. Nakai, T. Vreven, K. Throssell, J. A.Jr. Montgomery, J. E. Peralta, F. Ogliaro, M. J. Bearpark, J. J. Heyd, E. N. Brothers, K. N. Kudin, V. N. Staroverov, T. A. Keith, R. Kobayashi, J. Normand, K. Raghavachari, A. P. Rendell, J. C. Burant, S. S. Iyengar, J. Tomasi, M. Cossi, J. M. Millam, M. Klene, C. Adamo, R. Cammi, J. W. Ochterski, R. L. Martin, K. Morokuma, O. Farkas, J. B. Foresman and D. J. Fox, Gaussian, Inc., Wallingford CT, 2016.

(S4) M. Saliba, E. Unger, L. Etgar, J. Luo and T. J. Jacobsson, *Nat. Commun.*, 2023, **14**, 5445.